Surface Science xxx (2015) xxx–xxx

Contents lists available at ScienceDirect

Surface Science

journal homepage: www.elsevier.com/locate/susc

Interaction of CO with Pt_xAg_{1-x}/Pt(111) surface alloys: More than dilution by Ag atoms

K.M. Schüttler [a], L.A. Mancera [b], T. Diemant [a], A. Groß [b], R.J. Behm [a,*]

[a] Institute of Surface Chemistry and Catalysis, Ulm University, Albert-Einstein-Allee 47, D-89081 Ulm, Germany
[b] Institute of Theoretical Chemistry, Ulm University, Albert-Einstein-Allee 11, D-89081 Ulm, Germany

ARTICLE INFO

Available online xxxx

Keywords:
Bimetallic surface
Surface alloy
Chemisorption
Carbon monoxide
Temperature programmed desorption
IR spectroscopy
DFT calculations

ABSTRACT

We have investigated CO adsorption on structurally well-defined Pt_xAg_{1-x}/Pt(111) surface alloys, combining temperature-programmed desorption (TPD) and infrared reflection absorption spectroscopy (IRRAS) as well as density functional theory (DFT) based calculations. This is part of a systematic approach including previous studies of CO adsorption on closely related Pt(111)- and Pd(111)-based surface alloys. Following changes in the adsorption properties with increasing Ag content and correlating them with structural changes allow us to assign desorption features to specific adsorption sites/ensembles identified in previous scanning tunneling microscopy (STM) measurements, and thus to identify and separate contributions from different effects such as geometric ensemble effects and electronic ligand/strain effects. DFT calculations give further insight into the nature of the metal–CO bond on these bimetallic sites. Most prominently, the growth of a new CO desorption feature at higher temperature (~550 K) in the TPD spectra of Ag-rich surface alloys, which is unique for the group of Pt(111)- and Pd(111)-based surface alloys, is attributed to CO adsorption on Pt atoms surrounded by a Ag-rich neighborhood. Adsorption on these sites manifests in an IR band down-shifted to significantly lower wave number. Systematic comparison of the present results with previous findings for CO adsorption on the related Pt(111)- and Pd(111)-based surface alloys gains a detailed insight into general trends in the adsorption behavior of bimetallic surfaces.

1. Introduction

Bimetallic catalysts, i.e., supported catalysts with bimetallic nanoparticles, have attracted considerable interest in recent decades as they often show an improved activity and/or selectivity compared with the individual components [1–4]. A number of specific effects such as the geometric ensemble effect [5,6], site-blocking effects [7], or the electronic ligand [8–10] and strain [11,12] effects have been put forward to explain the improved performance of these catalysts. As an example, it is well known that the dilution of an active metal (like Pd or Pt) with an inert metal (like Au or Ag) enhances the selectivity and long-term stability in selective hydrogenation or other reactions like, e.g., vinyl acetate synthesis on PdAu catalysts [13]. This was explained by the reduced availability of larger active metal ensembles, which enable or enhance competing reactions. It should be noted that in particular the older models were strictly based on the correlation of the reaction kinetics with the composition of the catalyst particles, and direct experimental verification of these effects was hardly possible.

In modern catalysis research, where relative rates are often calculated within the framework of the Sabatier principle, based on the adsorption energies of the reaction educts, intermediates and products, and where the adsorption energies of the different species involved in a reaction are found to often vary in a correlated way between different catalyst materials [14], these adsorption energies are often calculated from the material or site dependent adsorption energies of a 'descriptor' species via the so-called scaling relations [15,16]. For bimetallic catalysts this means that various adsorption sites with different local compositions have to be considered for a comprehensive description of the reaction on these catalysts and for the identification of the active sites. Model studies along this way have been published recently for the electrocatalytic O_2 reduction on PtAu and PtRu bimetallic surfaces [17,18].

In an effort to better understand systematic trends in adsorption phenomena on bimetallic surfaces, we have investigated in previous years the adsorption of CO on structurally well-defined monolayer Pd_xAu_{1-x}/Pd(111) [19], Pd_xAg_{1-x}/Pd(111) [20–22] and Pt_xAu_{1-x}/Pt(111) [23] surface alloys, where the distribution of surface atoms was determined quantitatively by statistical evaluation of high resolution scanning tunneling microscopy (STM) images with chemical contrast [19,24–26]. Adsorption was investigated applying both experimental methods and density functional theory (DFT) based calculations. Completing this series of CO adsorption studies on closely related surface alloys, we here present results of a combined experimental and theoretical study on the interaction of CO with structurally well-defined Pt_xAg_{1-x}/Pt(111) surface alloys

* Corresponding author.
E-mail address: juergen.behm@uni-ulm.de (R.J. Behm).

http://dx.doi.org/10.1016/j.susc.2015.12.022
0039-6028/© 2015 Published by Elsevier B.V.

with systematically varied compositions. This is based on a detailed structural characterization by STM [27]. First experimental results on the formation of these surface alloys and characteristic electronic and CO adsorption properties at different stages of their formation were published recently [28]. An analysis of the structural stability of the Pt_xAg_{1-x}/Pt(111) surface alloys and related PtAg surfaces, based on STM data and DFT calculations, will be reported later [29].

Before entering into the presentation and discussion of our data, we will briefly summarize results from previous studies on the structural, electronic and adsorption properties of bimetallic PtAg surfaces and Pt_xAg_{1-x}/Pt(111) surface alloys. Although Pt and Ag are not bulk-miscible, it was already reported in the pioneering STM studies by Brune and Kern that intermixing of Ag deposits into a Pt(111) surface becomes possible upon heating; the onset of surface alloy formation was observed at ~620 K [30]. Further structural details including a quantitative description of the distribution of the two components in the surface alloy layer and of the abundance of small adsorption ensembles for varying compositions were recently derived in a detailed STM study [27]. In brief, this analysis showed a strong tendency towards phase separation in the surface alloy layer for the complete range of surface compositions [27]. The transfer of a measurable amount of Ag to the bulk upon annealing to temperatures below 850 K can be excluded on the basis of these measurements [27,30]. The electronic and adsorption properties of these surface alloys were studied by Strüber and Küppers using X-ray photoelectron spectroscopy (XPS) and temperature programmed CO desorption (CO TPD) measurements [31], respectively. In XPS, a uniform down-shift of the Ag($3d_{5/2}$) binding energy (BE) by ~0.4 eV compared with Ag(111) is found for all Ag contents up to 1 ML already before surface alloy formation. After surface alloy formation, an additional shift is detected whose amount varies with Ag surface concentration and takes a maximum additional decrease of ~0.3 eV for vanishing Ag content [31]. Although no complete CO TPD series were reported, the measurements showed the occurrence of an additional TPD peak at ~570 K, which was preliminarily attributed to CO adsorbed on atoms of a Pt cluster embedded in a Ag surrounding [31].

In the following we report on the CO adsorption properties of Pt_xAg_{1-x}/Pt(111) surface alloys, which were prepared by deposition of sub-monolayer amounts of Ag on Pt(111) at room temperature and subsequent heating to higher temperature. After a brief description of the experimental facilities and procedures (Section 2.1) and the computational details (Section 2.2), we will briefly summarize the most important structural characteristics of the Pt_xAg_{1-x}/Pt(111) surface alloys (Section 3.1.1), followed by the presentation of TPD and infrared reflection absorption spectroscopy (IRRAS) results for the CO adsorption on Pt_xAg_{1-x}/Pt(111) surface alloys with varying surface compositions (Sections 3.1.2 and 3.1.3). Section 3.2 comprises the results of systematic calculations of the CO adsorption energy on different relevant bimetallic surfaces. In Section 4.1 we discuss the experimental and computational results in a comprehensive way, focusing on trends in the CO adsorption properties induced by the varying local surface compositions. Finally, the data of the present study are compared with previous results on PtAu/Pt(111) [23], PdAg/Pd(111) [20–22] and PdAu/Pd(111) [19] surface alloys (Section 4.2).

2. Methods

2.1. Experimental part

The experiments were performed in an ultra-high vacuum (UHV) system (base pressure ~ 1×10^{-10} mbar) with facilities for TPD, IRRAS and XPS measurements, respectively. The system contains standard facilities for surface preparation, including an Ar^+ ion sputter gun and a Ag evaporator. The Pt(111) sample, which was used as substrate for the bimetallic surfaces, could be cooled by liquid nitrogen to ~90 K and heated by resistive heating. The surface was cleaned before each experiment by a cycle of Ar^+ sputtering (2 μA, 0.6 kV), oxygen treatment ($p_{O2} = 1 \times 10^{-7}$ mbar, 900 K), and annealing to 1200 K. Subsequently, surface order and cleanness were checked by CO TPD and XPS. Well-ordered and clean surfaces were identified by the absence of an additional feature at the high temperature edge of the main broad desorption peak in the CO TPD spectra, which is typical for desorption from defective surfaces [32,33] and the absence of any signal in the XP spectra not related to Pt. STM measurements on similarly prepared surfaces showed atomically smooth terraces (terrace width between 50 and 100 nm) separated by monoatomic steps [27].

In order to create the Pt_xAg_{1-x}/Pt(111) surface alloys, a sub-monolayer amount Ag was evaporated at room temperature (RT) from a resistively heated Knudsen cell (WA Technology), the deposition rate was ~0.05 monolayer (ML) min^{-1} (one monolayer refers to the surface atom density of Pt(111)). During Ag deposition, the background pressure remained in the lower 10^{-9} mbar range. After Ag deposition the sample was heated to 850 K for 1 min to complete surface alloy formation. The Ag concentration was determined by XP spectra using Mg K_α radiation for excitation and a hemispherical analyzer (CLAM2, VG Scientific) with a pass energy of 25 eV for detail and 50 eV for survey spectra. The Ag coverage was calibrated by a combination of CO TPD and XPS measurements, for details see the Supporting information.

For CO TPD and IRRAS experiments, dosing was done by backfilling the chamber via a glass tube (inner diameter 8 mm) pointing towards the sample (opening ~ 50 mm away). Due to this construction, the actual pressure during dosing is ~1.8 times higher than what is measured at the ion gauge, the exposure values were corrected for this. For the CO TPD experiments, the sample was exposed at 90 K to doses sufficient to reach saturation, which was obtained independently of the surface composition after exposure to 13.5 L CO (1 L = 1.33×10^{-6} mbar s). Subsequently, a linear heating ramp of 4 K s^{-1} was applied and the CO TPD spectra were recorded via a quadrupole mass spectrometer (Pfeiffer Vacuum, QMS 200). The mass spectrometer was shielded against desorption from edge areas or the sample holder by a cap with an aperture of 4 mm diameter [34]. Before a TPD run, the sample was positioned in front of the aperture, the distance between cap and sample was adjusted reproducibly by an electrical contact [35]. The IRRAS measurements were carried out at incidence and detection angles of 7° with respect to the surface plane using a mercury–cadmium–telluride (MCT) detector, the resolution was set to 4 cm^{-1}. Depending on the band intensities, between 1000 (for Pt(111)) and 4000 scans (for Ag-rich surfaces) were collected for one IR spectrum. Reference spectra of the CO_{ad} free surfaces were recorded after all CO was removed from the surface by heating to above the desorption temperature and subsequently cool-down to 200 K.

2.2. Computational details

Plane-wave DFT calculations were performed using version 5.3.3.4 of the VASP code [36], together with the Perdew–Burke–Ernzerhof (PBE) [37] and the revised-PBE (RPBE) [38] exchange–correlation functionals. The ionic cores are represented by projector augmented wave (PAW) potentials [39] as constructed by Kresse and Joubert [40,41]. The electronic one-particle wave functions are expanded in a plane-wave basis set up to a cutoff energy of 400 eV. This cutoff energy is expected to provide convergence better than 1 mRy (~13 meV) in eigenvalues for this kind of basis set. Spin polarization is not considered due to the non-spin-polarized nature of the system. Dipole moment correction is set up in order to account for effects derived of using asymmetric slabs. Scalar relativistic effects are already included from the parametrization at the basis set generation. Convergence criteria for the electronic self-consistency and the ionic relaxation are set to $1 \cdot 10^{-4}$ and $1 \cdot 10^{-5}$, respectively. A sufficiently large set of k-points was chosen in order to guarantee convergence.

First, the bulk energy (E_b) and bulk lattice parameter (d_b) of Pt and Ag were computed using an fcc unit cell and an $11 \times 11 \times 1$ Γ-centered k-point grid. Values obtained using PBE/PAW for the bulk lattice parameters

Please cite this article as: K.M. Schüttler, et al., Interaction of CO with PtxAg1−x/Pt(111) surface alloys: More than dilution by Ag atoms, Surf. Sci. (2015), http://dx.doi.org/10.1016/j.susc.2015.12.022

are 3.97 and 4.15 Å for Pt and Ag, respectively. These are in close agreement with the experimental values of 3.9231 Å and 4.0862 Å [42]. This yields nearest-neighbor distances of 2.81 Å and 2.93 Å for Pt(111) and Ag(111), respectively, which in the following are denoted as surface lattice parameters. Using RPBE, the bulk lattice parameters for Pt and Ag are 3.99 Å and 4.21 Å, and the nearest-neighbor distances for Pt(111) and Ag(111) are 2.82 Å and 2.98 Å, respectively. Note that RPBE yields compared with the experimental values a slightly larger overestimation of these parameters than PBE.

The bimetallic surfaces are represented by periodic slabs consisting of five monolayers. The vertical height of the three-dimensional unit cell has been set to an integer number of the surface lattice parameter, 10 d_s, which allows us to have a separation between slabs close to 18 Å in all cases. Geometry optimization of the various surface configurations has been carried out keeping the two bottom Pt(111) layers fixed at their corresponding bulk positions while the three upper layers are fully relaxed. We mainly use a (3 × 3) surface unit cell and perform geometry optimizations using a 3 × 3 × 1 Γ-centered k-point grid. For the various structures studied here we use the following notation: Pt_{5L} and Ag_{5L} denote pure platinum and silver slabs, Ag_{1L}/Pt(111) denotes a structure with one pseudomorphic silver overlayer above the Pt(111) substrate, and Pt_xAg_{1-x}/Pt(111) denotes surface alloys at the topmost layer created by replacing a certain fraction of Ag atoms by Pt atoms at the topmost layer of Ag_{1L}/Pt(111). $Ag_{2/3L}$/Pt(111) and $Ag_{2/3L}$/Ag(111) denote structures in which a row of silver atoms of the topmost overlayer in the 3 × 3 unit cell has been removed in order to simulate a step. Finally, PtAg/Ag_{nL}/Pt(111) are systems in which either one (n = 1) or two (n = 2) layers below the surface layer were replaced by Ag layers.

3. Results

3.1. Experimental results

3.1.1. Structural characterization

Before presenting the results of the current investigation of the CO adsorption properties, we briefly summarize the results of the previous high-resolution STM characterization of the Pt_xAg_{1-x}/Pt(111) surface alloys [27]. The samples were prepared in the same way as described above, by Ag deposition at RT, followed by annealing to allow for thermal intermixing of both metal components in the surface layer (surface alloy formation). In that study, atomically resolved STM pictures were recorded for various surface alloy compositions (see Fig. 1). From the digitized version of these images, the atom distribution was extracted, yielding information about the lateral short-range order as well as on the ensemble and ligand statistics.

First of all, that study confirmed the finding of the seminal STM studies of Röder et al. on Pt_xAg_{1-x}/Pt(111) surface alloy formation [30], who reported that Ag bulk diffusion can be neglected upon annealing to the temperatures necessary for 2D intermixing in the surface layer. Ag diffusion into the Pt bulk seems to be kinetically hindered under these conditions, although it would be thermodynamically favored by the large entropy contribution at the respective annealing temperature, which should easily counterbalance the larger surface energy of Ag compared with Pt [43]. This indicates that the substrate below the surface alloy layer remains pure Pt, and therefore vertical ligand effects, which might result from an introduction of Ag atoms into the surface near substrate, can largely be neglected. Second, both (sub-) monolayer Ag films on Pt(111) as well as monolayer Pt_xAg_{1-x}/Pt(111) surface alloys are pseudomorphic with respect to the substrate; no surface dislocations or reconstruction lines were observed in the structural characterization [27]. Therefore, increasing compressive strain can be expected with growing Ag concentration due to the incorporation of the larger Ag atoms into the Pt_xAg_{1-x} alloy layer which maintains the Pt(111) lattice parameter.

Third, quantitative evaluation of the STM images revealed a strong tendency for phase separation in these surface alloys, equivalent to a strong preference for homo-atomic neighborhoods and thus larger homo-atomic ensembles than obtained for a random distribution of the surface atoms. This is reflected by Warren–Cowley short-range order parameters which typically decreased continuously from about 0.3–0.5 for nearest neighbors to slightly above 0 for 5th nearest neighbors, depending on the Ag surface content (see also Supporting information) [27]. Comparison of the resulting surface atom distributions with those obtained for the closely related Pt_xAu_{1-x}/Pt(111), Pd_xAg_{1-x}/Pd(111) and Pd_xAu_{1-x}/Pd(111) monolayer surface alloys will be presented in the discussion in Section 4.2).

3.1.2. Temperature-programmed desorption

In the following, we present and briefly discuss the results of CO TPD measurements on the Pt_xAg_{1-x}/Pt(111) surface alloys with different Ag contents and, for comparison, on pure Pt(111). A more detailed discussion of the most important findings, which also takes into account the results of the DFT calculations (presented in Section 3.2), will follow in Section 4. The CO TPD spectra recorded after increasing CO exposures at 90 K are shown in Fig. 2.

The first panel (Fig. 2a) shows a series of CO TPD spectra recorded on pure Pt(111). After the smallest CO exposure (0.09 10^{-6} mars), a symmetric peak with a desorption maximum around 460 K appears. With increasing exposure, the desorption maximum shifts to lower temperature, indicating repulsive interactions between adsorbed CO molecules. At saturation coverage (black line) this results in an asymmetric desorption feature with its maximum around 370 K. The activation energy for desorption was determined at low CO coverage both by the leading edge analysis according to Habenschaden and Küppers [44] as well as by the Redhead method (assuming first order desorption and a pre-exponential factor of 10^{13} s^{-1}) [45], yielding 124 or 120 kJ mol^{-1}, respectively. (Note that an analysis of the leading edge of the spectra was possible only in that part of the experiments where the exposure was stepwise enhanced to improve the background pressure during the low exposure measurements.) These observations and results are in very good agreement with previous reports on the interaction of CO with Pt(111) surfaces [46–50]. The CO saturation coverage was normalized to 0.68 ML, the well-known value for CO chemisorption on Pt(111) at temperatures below 170 K [46].

The following panels (Fig. 2b–j) show sets of CO TPD spectra recorded on Pt_xAg_{1-x}/Pt(111) surface alloys with increasing Ag contents. In each of these panels, the black curve indicates the desorption spectrum from the CO_{ad} saturated Pt(111) for comparison. These spectra were recorded every day before Ag deposition and served as a daily CO_{ad} coverage calibration. Furthermore, they were used to verify the cleanness of the surface. The high CO_{ad} coverage red spectra refer to desorption from the CO_{ad} saturated surface alloys. Already after addition of 10% Ag (Fig. 2b), the CO_{ad} saturation coverage was found to decrease (see also below). Furthermore, a slight shift of the leading edge to lower temperatures ('low T shift'), as well as a high T shift of the trailing edge are resolved at CO_{ad} saturation compared with Pt(111). These slight changes in the peak shape are clearly related to the presence of the Ag atoms in the surface; similar effects were never observed in measurements on pure Pt(111). For surface alloys with Ag contents between 20% and 40% (Fig. 2c–e), the extension of the desorption peak to higher temperatures becomes much more pronounced. At the same time, the shape of the trailing edge changes for higher CO_{ad} coverage compared with pure Pt(111) and $Pt_{0.9}Ag_{0.1}$/Pt(111). Apparently, the surface becomes more and more inhomogeneous with regard to CO adsorption, containing on the one hand adsorption sites where adsorbed CO binds somewhat stronger, but keeping on the other hand also a (decreasing) fraction of Pt(111) like adsorption sites, which result in desorption in the main desorption feature. These trends are also apparent at lower CO_{ad} coverage: at 21% Ag content, the desorption features appear asymmetric already at medium coverage and at 40% even at low CO_{ad} coverage. At the same

Please cite this article as: K.M. Schüttler, et al., Interaction of CO with PtxAg1−x/Pt(111) surface alloys: More than dilution by Ag atoms, Surf. Sci. (2015), http://dx.doi.org/10.1016/j.susc.2015.12.022

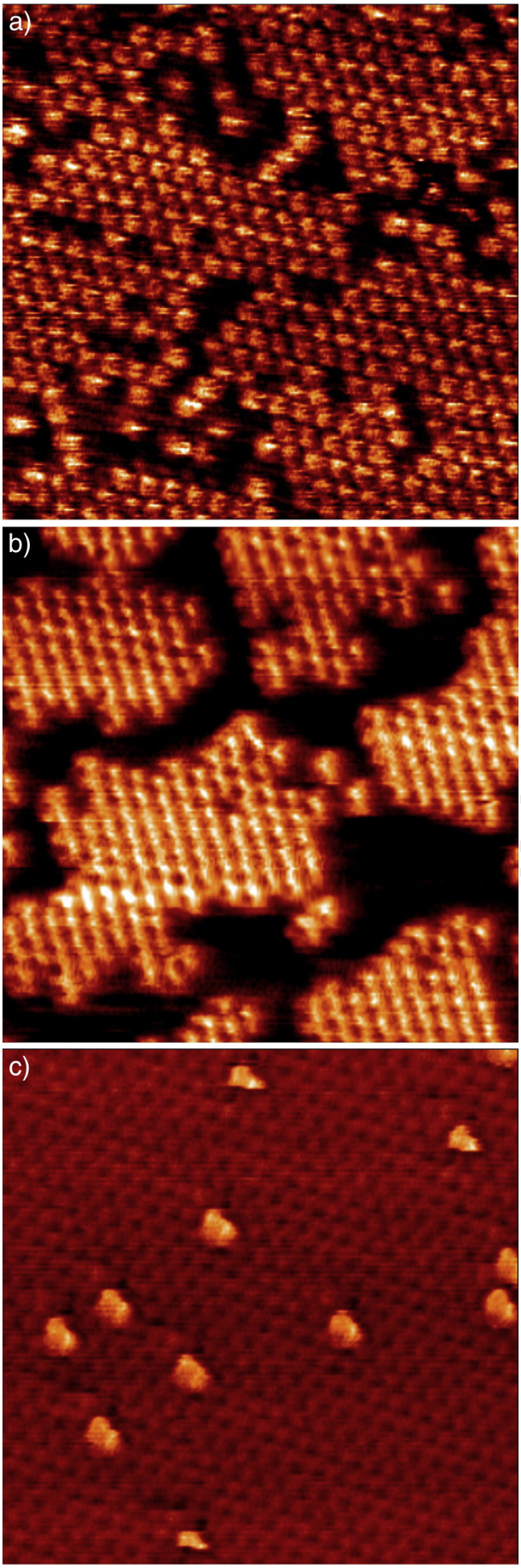

time the desorption peaks get significantly broader already after small CO exposures, i.e., the stabilized adsorption sites obviously show a variety of different adsorption energies, resulting in a continuous broadening of the CO desorption peak but no formation of a discrete desorption peak at the trailing edge. The latter would be expected if the stabilization resulted in one discrete value of the adsorption energy. This behavior changes significantly when the Ag content exceeds 50% (see Fig. 2f–j). At this point, the broadening of the CO desorption range to higher temperature stops, and a new discrete desorption feature is formed above 500 K, i.e., in a temperature range, where no desorption from well prepared Pt(111) surfaces occurs any more [33,46]. With 54% Ag (Fig. 2f), a small, but clearly visible distinct desorption feature appears at 540 K for all CO_{ad} coverages, while the majority of CO_{ad} still desorbs from Pt(111)-like sites. For further increasing Ag content, the high temperature desorption feature becomes more intense and develops into a very sharp peak in the desorption spectrum, while the intensity of the main desorption peak decreases successively. Eventually, for surface alloys with more than 80% Ag, the high temperature peak becomes the dominant feature of the desorption spectrum.

In order to illustrate the high T shift of the desorption maximum with increasing Ag content more clearly, the CO TPD spectra obtained after the smallest CO exposure ($\varepsilon_{CO} = 0.09$ mbar s) are collected in Fig. 3. Additionally, the temperatures of the peak maxima obtained on the different surfaces after the smallest CO exposure and after CO_{ad} saturation, respectively, are compiled in Fig. 4a. After the smallest CO exposure, a single symmetric desorption feature appears at 460 K for pure Pt(111). The desorption maximum shifts to ~485 K for surface alloys with 20–40% Ag. For 54% Ag, with the enhanced formation of the new high-temperature desorption feature, the main desorption feature shifts back to ~480 K and the high-temperature desorption feature appears at significantly higher temperature (~540 K). A further increase of the Ag concentration in the layer induces a slight upshift of the high T feature (to ~560 K), while the main desorption feature shifts only marginally to lower temperature.

The activation barriers for desorption (Fig. 4b) determined by the Redhead method or via the leading edge analysis (see above) for the lowest exposure reproduce this trend. Only for very high Ag contents, the value of the leading edge analysis seems to disagree with the findings of the Redhead analysis. Here it should be noted that while both methods assume a homogeneous surface, they are differently affected by the presence of inhomogeneous surfaces, due to the fact that they focus on different desorption ranges and therefore coverage regimes in each spectrum (onset of desorption vs. maximum desorption rate).

Another interesting feature of the TPD spectra is their growth behavior with increasing CO exposure. Both the main desorption peak and the high temperature feature grow simultaneously, indicating that the adsorption sites corresponding to these two peaks are populated at the same time and not sequentially, as would be expected from an energetic point of view. Such behavior is most easily explained by a physical isolation of the two types of adsorption sites, as it will occur for Pt islands separated by a "sea" of weakly binding Ag atoms, which does not allow for surface diffusion of CO_{ad} between the two Pt islands.

For smaller Ag contents up to 21%, the slight shift of the leading edge at saturation coverage to lower temperature, by up to 10 K, which we had already described for the surface alloy with 10% Ag, still appears. Since at CO_{ad} saturation also repulsive adsorbate–adsorbate interactions come into play in addition to electronic ligand and strain effects, an unambiguous identification of the reasons for this shift is difficult. Starting from intermediate Ag content, around 30%, the leading edge at CO_{ad} saturation coverage shifts continuously back to higher temperatures compared with Pt(111). This up-shift may be due to two different effects,

Fig. 1. Atomically resolved STM images with chemical contrast for surface alloys with increasing Ag contents. Surface composition and tunneling parameters are: a) 25% Ag, $I_T = 71$ nA; $V_T = 8.5$ mV; b) 46% Ag, $I_T = 71$ nA; $V_T = 5.5$ mV; and c) 95% Ag, $I_T = 71$ nA; $V_T = 7.0$ mV.Images are taken from reference [27].

Please cite this article as: K.M. Schüttler, et al., Interaction of CO with PtxAg1−x/Pt(111) surface alloys: More than dilution by Ag atoms, Surf. Sci. (2015), http://dx.doi.org/10.1016/j.susc.2015.12.022

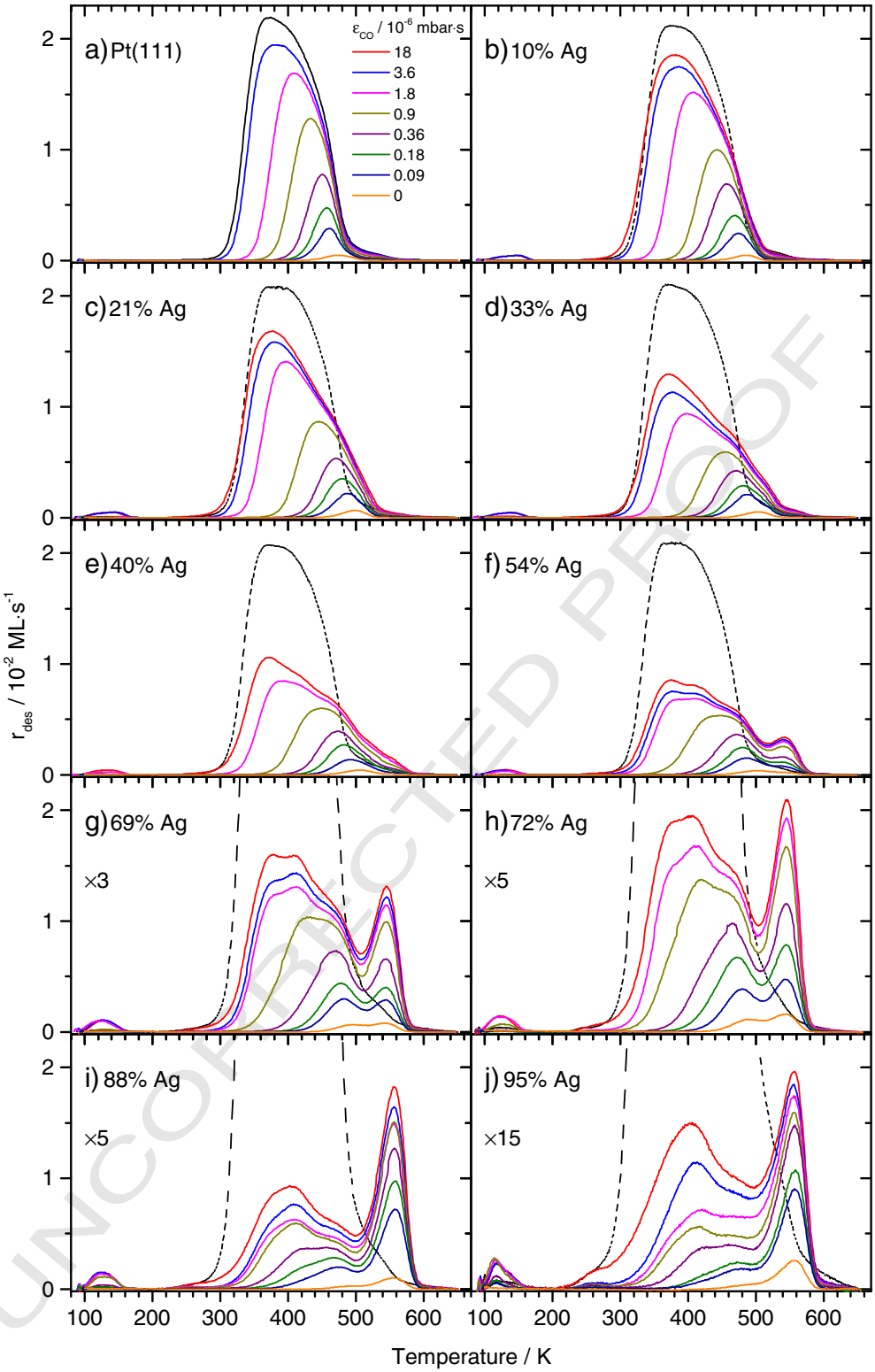

Fig. 2. CO TPD spectra recorded on pure Pt(111) (panel a) and on various Pt_xAg_{1-x}/Pt(111) surface alloys with increasing Ag content (panels b–j). Exposures are given in the first panel (increasing exposure form bottom to top); the (bottom) orange line reflects adsorption from the residual gas during cool-down of the sample. For each surface alloy, the desorption spectrum of pure Pt(111) is included as dashed black line. (For interpretation of the references to color in this figure legend, the reader is referred to the web version of this article.)

(i) a stabilization of CO adsorbed on Pt sites by neighboring Ag surface atoms and/or (ii) decreasing CO_{ad}–CO_{ad} repulsions due to the increased presence of 'empty' Ag surface sites.

The CO_{ad} saturation coverage (Fig. 4c) seems to decrease — within the error bars — almost linearly with the Ag content, indicating that the overall CO saturation coverage per Pt surface atom does not change significantly with Ag content. This observation seems to be surprising, since the CO_{ad} saturation coverage for Pt(111) at low temperature under UHV conditions is 0.68 ML [46], while at least for Ag-rich surface alloys with a large number of smaller Pt ensembles, e.g., monomers, dimers and trimers, which are surrounded by Ag atoms, one might expect that due to decreasing steric limitations the CO_{ad} saturation coverage

Please cite this article as: K.M. Schüttler, et al., Interaction of CO with PtxAg1−x/Pt(111) surface alloys: More than dilution by Ag atoms, Surf. Sci. (2015), http://dx.doi.org/10.1016/j.susc.2015.12.022

per Pt surface atom is higher, approaching in the end a value of one CO per Pt surface atom. Apparently, these effects are not significant within the precision of the measurements. We expect that similar to the case of PtAu/Pt(111) surface alloys [23], which also show a considerable segregation of homo-atomic species in the surface alloy layer [26], notable deviations of the CO_{ad} saturation coverage from a linear behavior are precluded by the fact that the tendency for segregation results in relatively large Pt ensembles in the mixed surface layer already for very small Pt concentrations.

Finally, for all surface alloys we observed an additional, very small ($\theta_{CO} < 0.01$ ML) desorption feature right after the beginning of the temperature ramp at very low temperature (Fig. 5) as soon as the exposure exceeds the dose necessary to saturate the Pt sites of the surfaces (desorption T > 300 K). An exposure of $3.6 \cdot 10^{-6}$ mbar s was sufficient in all cases to saturate this peak. This feature was never observed in the case of a CO_{ad} saturated unmodified Pt(111) surface (cf. dashed black line in Fig. 5) and is therefore clearly a unique feature of the Pt_xAg_{1-x}/Pt(111) surface alloys. From the desorption temperature it may be concluded, that this feature is related to CO desorption from Ag sites, since no desorption from Pt sites can be observed below 300 K. It is known that CO desorption from Ag(111) terrace sites occurs around 50 K [51], while for stepped surfaces another desorption peak at higher temperature due to desorption from the step sites appears at 80–90 K (Ag(211) [52]). From the desorption temperature of ~140 K in the case of the present bimetallic surfaces, a stabilization of CO adsorption on Ag atoms in contact with the Pt substrate may be inferred. This point will be addressed in more detail in Sections 3.2.3 and 3.2.4.

The TPD series were also used to characterize the CO adsorption kinetics for the various surface alloys and for pure Pt(111) as a reference. Differential sticking coefficients (Fig. 6) were obtained by calculating the differences between CO coverages θ and exposures ε for CO coverage — CO exposure pairs with increasing CO exposure and dividing Δθ obtained this way by Δε. The initial sticking coefficients s_0 (Fig. 6, inset) were determined by extrapolation of the differential sticking coefficients to zero CO coverage. The initial sticking coefficient of Pt(111) was normalized to the literature value of 0.84 determined in a molecular beam experiment [53] to correct for the difference between nominal pressure and actual pressure at the sample (see experimental part). Instead of a linear decrease of the differential sticking coefficients with increasing CO coverage, which would be expected in the case of simple first-order Langmuir adsorption kinetics, all surfaces show a behavior where the sticking coefficient remains at rather high values, and decays only at coverages close to saturation. Such behavior can be described by the Kisliuk model for precursor adsorption [54] (see the thin lines in Fig. 6). Similar adsorption kinetics were already reported before for CO adsorption on Pt(111) [53] or other late transition metals (e.g., Pd(111) [55], Ru(0001) [56]), but also for other bimetallic surfaces (e.g., PtSn/Pt(111) [57] or PtAu/Pt(111) [23] surface alloys). Taking the initial sticking coefficients (Fig. 6, inset), it is interesting to note that s_0 stays about constant (at ~ 0.84) over a wide range of surface compositions. Only for the surface alloy with 75% Ag we find a slight decrease to a value of 0.72. These findings clearly imply that Ag sites act as intrinsic precursor sites for CO adsorption at 90 K. CO molecules arriving at Ag surface atoms of the alloy surfaces can travel from there to free Pt surface sites. The lifetime of the precursor state (CO_{ad} bound to Ag atoms) at this adsorption temperature must be sufficiently long that for a wide range of Ag contents the variation of the Ag surface content does not affect s_0. A similar effect was first described by Xu and Koel for PtSn/Pt(111) surface alloys [57] and later also observed by our group for PtAu/Pt(111) [23] and PdAg/Pd(111) [21] surface alloys. In the two latter cases, however, the effect was not so pronounced.

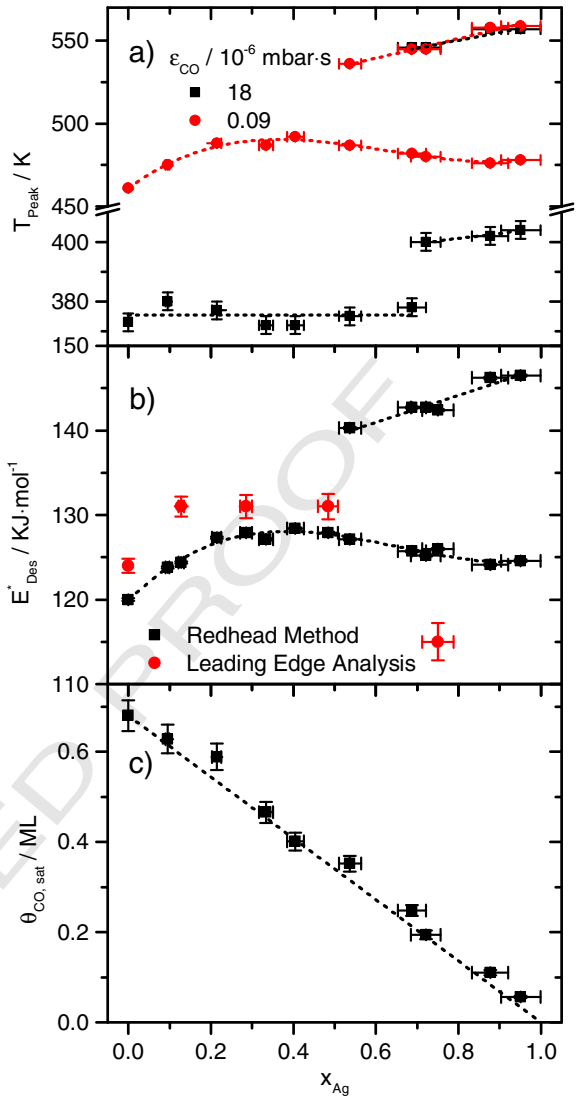

Fig. 4. a) Temperature of the CO TPD peak maximum both after very small and after the largest exposures ($\varepsilon_{CO} = 0.09$ and 18×10^{-6} mbar s) recorded on Pt(111) and on various Pt_xAg_{1-x}/Pt(111) surface alloys. The second data points refer to the high temperature peak once it is observed. b) Activation barriers for desorption from Pt(111) and the various surface alloys determined by the Redhead method and by the leading edge analysis. c) CO_{ad} saturation coverage for Pt(111) and various surface alloys. (Lines serve to guide the eye.)

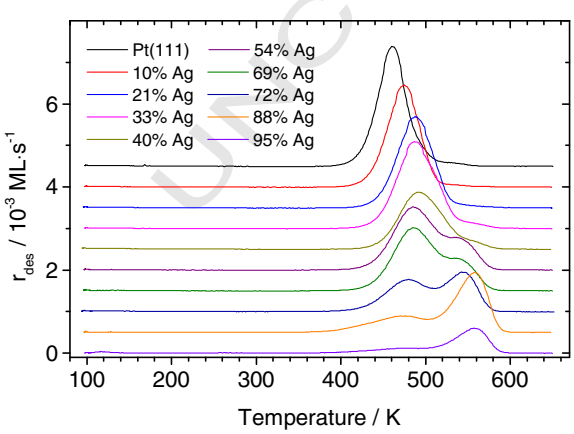

Fig. 3. CO TPD spectra recorded after the lowest CO exposure ($\varepsilon_{CO} = 0.09 \times 10^{-6}$ mbar s) on Pt(111) (topmost, black line) and on various Pt_xAg_{1-x}/Pt(111) surface alloys with increasing Ag content (top to bottom). (For interpretation of the references to color in this figure legend, the reader is referred to the web version of this article.)

Please cite this article as: K.M. Schüttler, et al., Interaction of CO with PtxAg1−x/Pt(111) surface alloys: More than dilution by Ag atoms, Surf. Sci. (2015), http://dx.doi.org/10.1016/j.susc.2015.12.022

3.1.3. IR spectroscopy

In this section, we present results from IR measurements on surface alloys of varying compositions and on the unmodified Pt(111) as reference. The IR spectra were recorded both after increasing CO exposures up to CO_{ad} saturation at low temperature (90 K) and after CO_{ad} saturation at 90 K, followed by stepwise heating to temperatures sufficient for sequential CO desorption (viz., 200, 350, 400, 450 and 500 K).

Starting with the IR measurements on pure Pt(111) (Fig. 7a), adsorption of a small amount of CO at 90 K results in a single IR band at 2091 cm^{-1}, reflecting on-top adsorbed CO. With increasing coverage, this band shifts to higher wavenumbers. Above $\theta = 0.33$ ML, an additional broad band appears at 1853 cm^{-1}, which is attributed to bridge-adsorbed CO. With further increasing CO_{ad} coverage, the first band continues to shift, reaching 2105 cm^{-1} at saturation, and also the lower frequency band shifts to lower wavenumber. These IR spectra (as well as the CO TPD spectra presented before) are in full agreement with previous reports on CO adsorption on Pt(111) [46,47,53,58–64].

For CO adsorption on the surface alloys, the band related to bridge-bonded CO_{ad} which forms at high CO_{ad} coverage, loses rapidly in intensity with increasing Ag surface content. Since the occupation of this adsorption site is likely to be correlated with the appearance of long-range ordered adsorbate layers (with $c(4 \times 2)$ or larger unit cells) at higher CO_{ad} coverages, we explain the disappearance of this peak by the decreasing formation of these adlayer phases on the surface alloys, which lack large contiguous Pt surface areas. A similar behavior of the adlayer was observed also on PtAu/Pt(111) surface alloys [23].

Focusing now on the band related to on-top adsorbed CO_{ad}, we find this band at lower wavenumber, with peaks at 2079 and 2071 cm^{-1}, and less sharp for the surface alloy with the smallest Ag content (8%) after the smallest CO exposure. The broadening indicates an increasing inhomogeneity of the surface alloys, which leads to the occupation of adsorption sites with slightly different vibrational properties. With increasing CO exposure/coverage, the peak shifts to a higher wavenumber and eventually arrives at 2103 cm^{-1} for CO_{ad} saturation, indicating that Pt(111) like sites increasingly dominate at higher CO_{ad} coverages.

For higher Ag surface contents, from 20% Ag on, bands related to on-top adsorption remain split into different signals also at higher coverage. Generally, the bands appear at increasingly lower wavenumbers with increasing Ag content, and this goes along with a drastic loss in IR intensity, both compared with unmodified Pt(111) (see above), but also in comparison with CO_{ad} on PtAu/Pt(111) [23]. In combination with the pronounced band broadening, this does not allow any more the determination of the wavenumber of the bands exactly. Therefore, we will only mention the wavenumber with the maximum intensity.

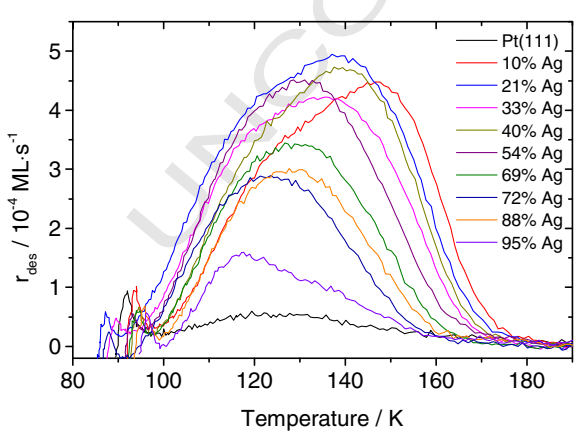

Fig. 5. Magnified presentation of CO TPD spectra recorded on Pt(111) (bottom black line) and on various Pt_xAg_{1-x}/Pt(111) surface alloys (composition see figure, increasing Ag content approximately from bottom to top) after the largest CO exposure ($\varepsilon_{CO} = 18 \times 10^{-6}$ mbar s), focusing on the low temperature feature. (For interpretation of the references to color in this figure legend, the reader is referred to the web version of this article.)

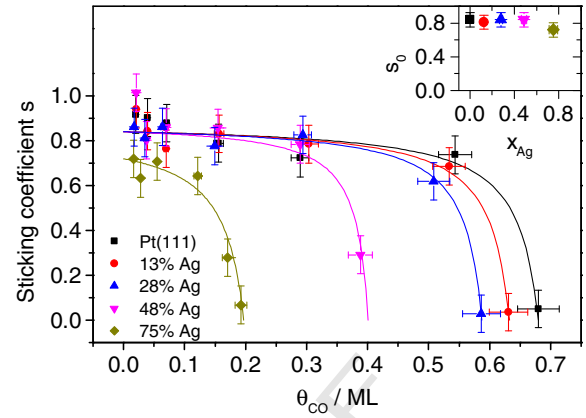

Fig. 6. Differential sticking coefficients s determined from the CO TPD spectra recoded on Pt(111) and on various Pt_xAg_{1-x}/Pt(111) surface alloys. Lines indicate fits according to the Kisliuk model (decreasing saturation coverage with increasing Ag content). Inset: initial sticking coefficients obtained by extrapolation of differential sticking coefficients to zero CO coverage.

Nevertheless, the shift of these bands to lower wavenumbers is large enough to be clearly detectable. For surface alloys with 20 and 30% Ag (Fig. 7c–d), the main IR features after the smallest CO exposure are located at 2068 and 2058 cm^{-1}, respectively. With increasing coverage, a dominant peak appears at higher wavenumbers whose position is close to that on Pt(111), but shifted to slightly lower wavenumber, reaching 2099 and 2096 cm^{-1} at CO_{ad} saturation. The bands at lower wavenumber persist after CO_{ad} saturation for both surfaces as a shoulder at the lower wavenumber side of the main IR peak, their relative contribution grows with increasing Ag content. As a consequence, the broad feature at ~2080 cm^{-1} obtained after CO_{ad} saturation for a surface alloy with 47% Ag is a convolution of the former main peak and this shoulder.

At 61% Ag surface content the IR bands show again a constant shift to higher wavenumber with increasing coverage, starting with a double band at 2055 and 2046 cm^{-1} at low coverage and ending up with a very wide band at 2070 cm^{-1}. At high coverage, a very small IR band at 2028 cm^{-1} can be observed, which would not have been considered as a band from these spectra, but will become important later on. With 74% Ag, the IR bands appear even wider and weaker in intensity. Again, a very small band can be observed at 2025 cm^{-1} for all coverages.

In total, these IR spectra clearly indicate that with increasing Ag surface content the IR bands shift to lower wavenumbers. In the commonly used Blyholder picture of CO adsorption on late transition metals [65], this indicates a stronger contribution of the $2\pi^*$ back-donation to the Pt–CO bond, which is often correlated with an increasing CO binding strength. This conclusion is in good agreement with the CO TPD data, which also showed an increased CO adsorption energy. The frequency range covered by the bands related to the on-top adsorbed CO is significantly larger than in the case of PtAu/Pt(111) surface alloys. Hence, Ag surface atoms seem to have a much stronger effect on the $2\pi^*$ back donation from the neighboring Pt surface atoms than Au surface atoms. This is paralleled by the TPD results, which also show a stronger influence of Ag ligand atoms than Au on the CO adsorption on adjacent Pt sites.

From the above data it was essentially not possible to correlate a specific IR band with the high temperature desorption peak in the TPD spectra. Considering its intensity (e.g., 7% of a ML for a surface alloy with 82% Ag) and relatively small peak width, which points to a rather large uniformity of the corresponding adsorption sites, one would expect a visible IR signal. Among other reasons this may be related to an insufficient ordering, precluding the population of the adsorption sites related to this desorption peak during adsorption at 90 K. Therefore we performed an additional series of IR measurements, where different CO coverages were not produced by dosing different amounts of CO at

Please cite this article as: K.M. Schüttler, et al., Interaction of CO with PtxAg1−x/Pt(111) surface alloys: More than dilution by Ag atoms, Surf. Sci. (2015), http://dx.doi.org/10.1016/j.susc.2015.12.022

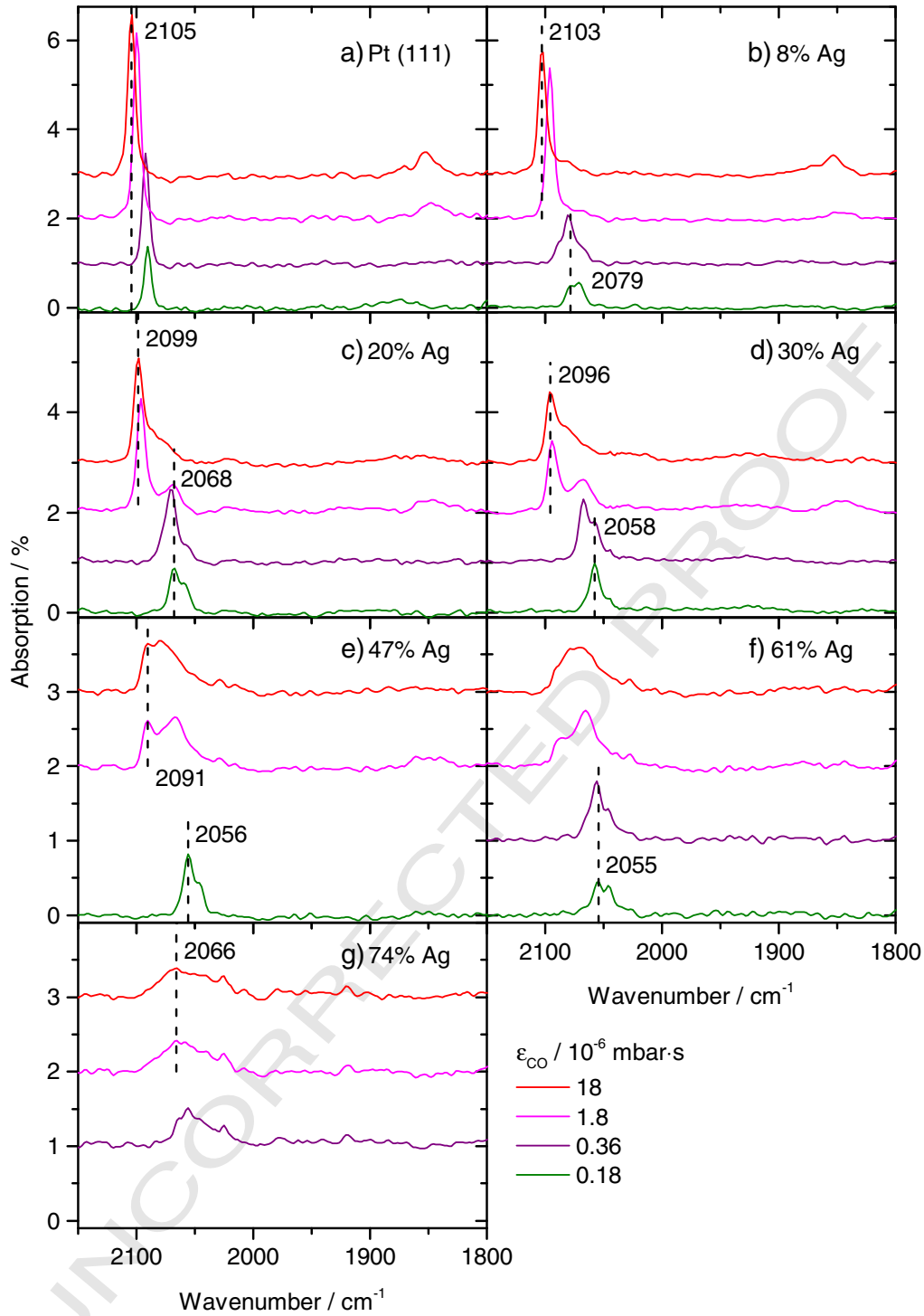

Fig. 7. IRRA spectra recorded on Pt(111) (a) and on various Pt_xAg_{1-x}/Pt(111) surface alloys (b–g) after different CO exposures at 90 K (increasing exposure from bottom to top).

90 K, but by saturating the surface with CO at 90 K and subsequent stepwise annealing in order to sequentially desorb CO in the order of increasing binding strength.

Spectra recorded after different annealing steps and on different surfaces are shown in Fig. 8. Starting with unmodified Pt(111), we find directly after CO_{ad} saturation at 90 K a sharp band at 2105 cm^{-1} and a less intense band at 1853 cm^{-1}, as described before (see above), which were attributed to on-top and bridge-bonded adsorbed CO. With increasing heating temperature, the band at 2105 cm^{-1} first grows in intensity. After heating to 400 K it reaches the maximum intensity and shifts to a slightly lower wavenumber. This can be explained by increased ordering due to annealing of the adsorbate layer and by weaker repulsive interactions due to reduced CO coverage after the onset of CO desorption (350 K). After the last heating step to 450 K, the peak loses much of its intensity and shifts to 2089 cm^{-1}. The band attributed to bridge-adsorbed CO reaches its maximum intensity after heating to 350 K and has completely vanished after heating to 400 K. This together with the beginning shift of the band of linearly adsorbed CO suggests that after heating to 350 K the compressed structure is transformed into the c(4 × 2) structure and after heating to 400 K into the $(\sqrt{3} \times \sqrt{3})R30°$ structure [46,47,53]. The much higher intensity of the band attributed to bridge adsorbed CO compared with the spectra

Please cite this article as: K.M. Schüttler, et al., Interaction of CO with PtxAg1−x/Pt(111) surface alloys: More than dilution by Ag atoms, Surf. Sci. (2015), http://dx.doi.org/10.1016/j.susc.2015.12.022

recorded after adsorption at 90 K points to an improved ordering of the adlayer.

For small and medium Ag surface contents, from 10 to 40%, the IR spectra are very similar to those obtained after different CO exposures at low temperature, indicating that the adlayer structure formation is fast and not kinetically hindered. After adsorption at 90 K, the spectra are still similar to those of Pt(111), except for a slight shift of the main band to a lower wavenumber, which becomes more pronounced with increasing Ag content, and the appearance of the shoulder at a lower wavenumber. With decreasing CO_{ad} coverage, roughly after heating to 400 K, however, there is a clear change and the band has shifted now to a much lower wavenumber than obtained on pure Pt(111), indicating the depopulation of Pt(111) like sites.

This behavior changes for surface alloys with more than 40% Ag. After adsorption at 90 K, only a wide IR band can be observed. While after adsorption and after annealing to lower temperatures the spectra still look rather similar, higher temperature annealing and especially the last annealing step to 500 K result in significant changes. A new IR band appears at low wavenumbers, lower than those observed during adsorption after the smallest CO dose. In our interpretation this annealing step allows the selective probe of the stabilized CO_{ad} molecules, which will desorb in the high temperature desorption feature. All CO adsorbed on Pt(111) like sites has already desorbed at this temperature. Therefore, the band between 2030 and 2025 cm^{-1} appearing in these spectra is clearly related to CO_{ad} species adsorbed on stabilized sites which are related to the high-temperature desorption peak. The very low wavenumber indicates a strong stabilization of adsorbed CO, which is in good agreement with TPD results, and, compared with other bands, its very defined shape also supports the uniformity of these adsorption sites already concluded from the width of the corresponding TPD peak.

Overall, the IR measurements confirm the formation of a new Pt–CO adsorption site, which had been detected in the TPD spectra as high temperature desorption feature.

3.2. Theoretical results

Pt_xAg_{1-x}/Pt(111) surface alloys with low Pt content can be approximated by small Pt ensembles partly surrounded by Ag atoms in the topmost layer on a Pt bulk. For the present calculations, we considered Pt monomers, dimers and compact Pt trimers as adsorption ensembles, which are represented by Pt_1Ag_8/Pt(111), Pt_2Ag_7/Pt(111), and Pt_3Ag_6/Pt(111) structures in a (3×3) unit cell. They result from substituting 8, 7, or 6 Pt surface atoms by Ag atoms at the pure Pt(111) surface in the unit cell, or conversely, from substituting 1, 2, or 3 Ag atoms by Pt atoms per unit cell in a pseudomorphic Ag monolayer on Pt(111) (Ag_{1L}/Pt(111)). In a first order approximation these structures can also be used as model for surfaces with higher Pt content, assuming that the additional changes in the CO adsorption energy when going to larger ensembles, due to strain and ligand effects, will not be too large. These aspects will be discussed also in Section 4.1.

It is known that first-principles calculations do not properly describe the adsorption site preference for CO on Pt(111): while experimentally CO was found to adsorb in on-top positions of Pt(111) (at low CO_{ad} coverages), most DFT calculations predict adsorption in the fcc hollow site to be most stable. This problem has been widely discussed by Feibelman et al. [66] and later by other authors [67–70]. This discrepancy between theory and experiment can be rationalized from the fact that first-principles calculations within the generalized gradient approximation (GGA) considerably underestimate the energy gap between the highest occupied molecular orbital (HOMO) and the lowest unoccupied molecular orbital (LUMO) (see ref. [71] and references therein). For the present study, where we are mainly interested in systematic variations of the CO adsorption energy with varying compositions of the adsorption ensemble, more specifically in the influence of strain and ligand effects, the site effects described above are less decisive. Therefore, despite the known difficulties of the commonly used DFT functionals to describe CO adsorption on Pt(111) properly, we used PBE and RPBE functionals to describe CO adsorption on the Pt_xAg_{1-x}/Pt(111) surface alloys. We did not include van der Waals interactions, since they are usually not crucial in the description of strongly adsorbed molecules such as CO. In a previous study, we had shown that the use of RPBE functionals leads to values of the CO adsorption energy on Pd(111) which are closer to experimental results than those obtained from the more commonly used PBE functional, while at the same time both functionals provide similar trends [22]. Similar trends were obtained also for both functionals when studying CO adsorption on Pd_xAg_{1-x}/Pd(111) surface alloys [22]. Finally, it should be noted that based on the experimental results, we did not consider CO adsorption on Ag surface atoms on the bimetallic surfaces.

3.2.1. The CO/Pt(111) system

Table 1 shows adsorption energies for the CO molecule adsorbed in different sites of the Pt(111) surface (Fig. 9a), calculated using PBE/PAW and RPBE/PAW; the adsorbate structures considered at different CO_{ad} coverages are illustrated in Fig. 9b. CO adsorption energies obtained with RPBE are in general smaller (by 0.3 to 0.4 eV) than those obtained using PBE. Furthermore, although both DFT functionals lead to the same adsorption site at low coverages (1/9 ML), they provide different results at intermediate and high coverages. Using RPBE for coverages of $\theta_{CO} = 1/3$ and $\theta_{CO} = 2/3$, the CO molecules adsorb in the bridge and the on-top site, respectively, while the use of PBE predicts adsorption in threefold hollow sites for all coverages. Although some differences in the energy values are small (~0.01 eV), they are still in the range of the chemical accuracy of DFT calculations, thus allowing us to identify preferred adsorption sites.

It has been shown in various experimental reports that the site preference for CO adsorption on Pt(111) varies with the CO coverage (see also [66]): on-top adsorption is favored at low coverages up to $\theta_{CO} = 1/3$ ML ($(\sqrt{3} \times \sqrt{3})R30°$ structure) [47]. Beyond that coverage, also adsorption in bridge sites occurs, with up to 50% of the CO molecules adsorbed in bridge sites at $\theta_{CO} = 0.5$ ML ($c(4 \times 2)$ structure) [47,62]. In the high coverage regime exceeding $\theta_{CO} = 0.5$ ML, where more complex adlayer structures are formed, the fraction of CO molecules adsorbed in bridge sites decreases again [62].

3.2.2. The CO/Ag(111) system

For comparison, we also calculated adsorption energies for similar sites and CO_{ad} coverages as described before for CO adsorption on Ag(111). The resulting values are collected in Table 2. Similar to adsorption on Pt(111), CO adsorption energies obtained with RPBE are in general smaller (by 0.2 to 0.4 eV) than those obtained using PBE. Compared with adsorption on Pt(111), CO adsorption energies on Ag(111) are very small and sometimes even assume positive values. These findings agree perfectly with results from experimental studies, where CO adsorption on Ag(111) was found to be extremely weak, with a desorption temperature below 60 K, corresponding to an adsorption energy of about 0.2 eV [51]. In this case, values obtained using PBE functionals seem to agree better with experimental data. Interestingly, RPBE calculations reveal very large differences, at least on a relative scale, between adsorption in hollow sites and on-top and bridge sites, respectively, at the lowest coverage. Furthermore, they reflect distinct and rather erratic coverage effects.

In order to elucidate also effects caused by CO adsorption at a defect Ag site, e.g., at a step in the Ag(111) surface, we removed a row of atoms along the <010> direction in the (3×3) unit cell and denote this as $Ag_{2/3L}$/Ag(111) surface. We located a CO molecule at different sites at or close to the step edge, at a CO_{ad} coverage of $\theta_{CO} = 1/9$, as schematically indicated in Fig. 9c. The sites are located at the upper level of the step edge. The adsorption energies calculated for adsorption on the different sites are collected in Table 3. Adsorption in on-top and bridge sites at the lower level of the step edge was not explored. When locating

Please cite this article as: K.M. Schüttler, et al., Interaction of CO with PtxAg1−x/Pt(111) surface alloys: More than dilution by Ag atoms, Surf. Sci. (2015), http://dx.doi.org/10.1016/j.susc.2015.12.022

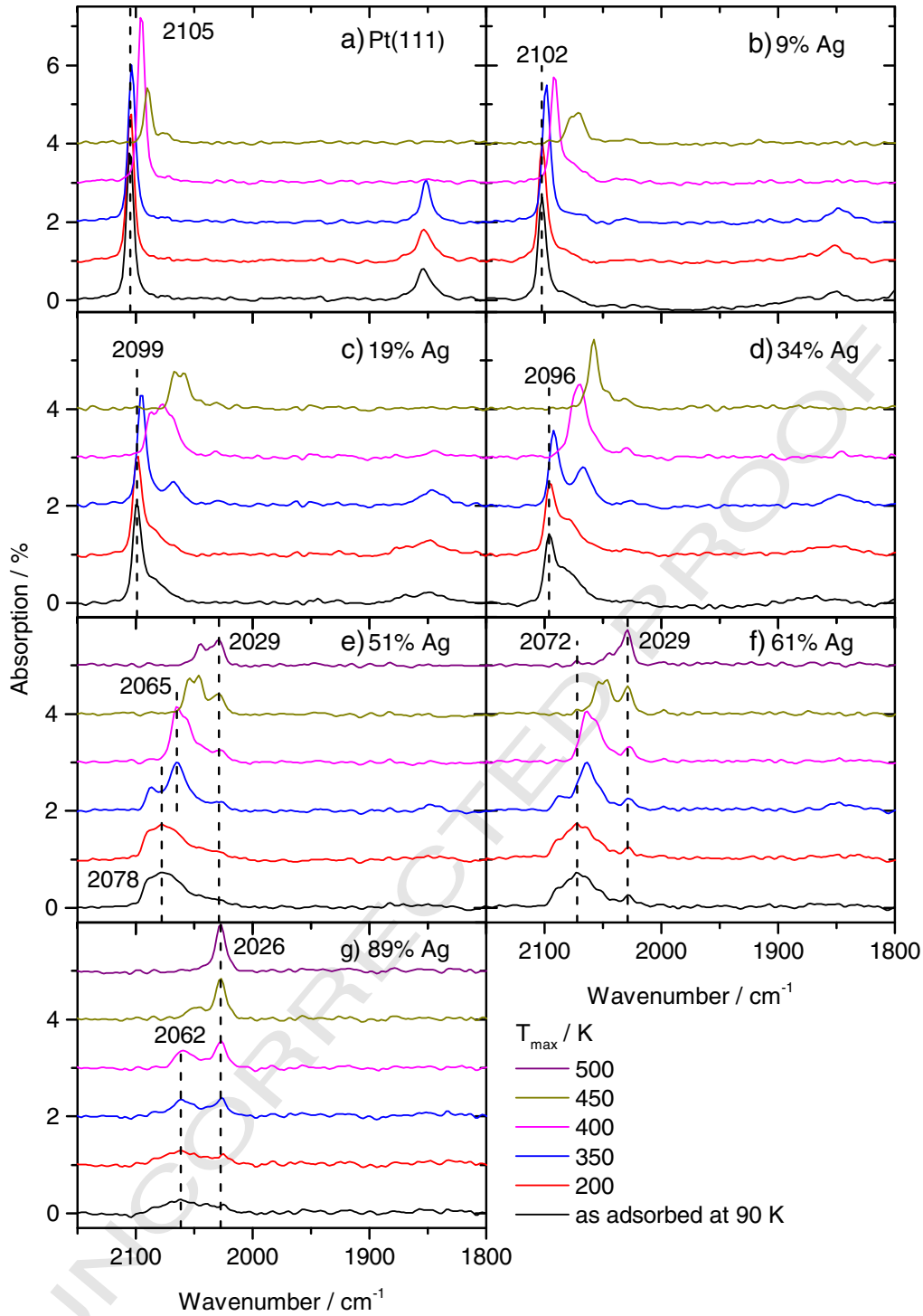

Fig. 8. IRRA spectra recorded on Pt(111) (a) and on various Pt_xAg_{1-x}/Pt(111) surface alloys (b–g) after CO_{ad} saturation at 90 K (bottom) and stepwise heating to successively desorb CO again. IR measurements were performed after cool-down to 200 K after each heating step (increasing temperature from bottom to top).

the CO molecule at the upper level, even in a threefold site at the edge, downward motion to the lower level position did not take place. Instead, the molecule either tilted close to the Ag atom or it moved to an on-top or bridge position at the upper level. Using PBE, the CO molecule adsorbs preferentially in the on-top sites at the upper level of the step edge, with adsorption energies in the range of −0.36 to −0.41 eV, followed by adsorption in bridge sites also at the upper level of the step edge with values in the range of −0.33 to −0.38 eV. Using RPBE, adsorption in on-top sites on the upper level is preferred again, with adsorption energies in the range of −0.15 to −0.19 eV, followed by adsorption in bridge sites with adsorption energies in the range of −0.06 to −0.10 eV. Overall, in agreement with previous experimental findings for stepped Ag surfaces [52], adsorption on the upper terrace step sites is more stable than on terraces or on lower terrace step sites.

3.2.3. The CO/Ag_{1L}/Pt(111) system

In order to gain more information on CO adsorption on extended Ag monolayer areas in the surface of the Pt_xAg_{1-x}/Pt(111) surface alloys, we furthermore calculated adsorption energies for CO adsorption on a Ag_{1L}/Pt(111) surface, i.e., on a Ag monolayer deposited on the Pt(111)

Please cite this article as: K.M. Schüttler, et al., Interaction of CO with PtxAg1−x/Pt(111) surface alloys: More than dilution by Ag atoms, Surf. Sci. (2015), http://dx.doi.org/10.1016/j.susc.2015.12.022

Table 1
Adsorption energies (in eV) calculated using PBE/PAW and RPBE/PAW for CO adsorption on Pt(111) for different CO_{ad} coverages. The labels T, fcc, hcp, and B denote adsorption in on-top, hollow-fcc, hollow-hcp, and bridge sites, respectively. Bold values denote the preferential adsorption site in each case as determined by DFT calculations (note that this assignment differs with experimental results ('Pt puzzle').

	PBE/PAW			RPBE/PAW		
Θ_{CO}	1/9	1/3	2/3	1/9	1/3	2/3
T	−1.81	−1.73	−1.33	−1.52	−1.44	**−0.99**
B	−1.88	−1.80	−1.35	−1.54	**−1.46**	−0.96
fcc	**−1.91**	−1.81	**−1.39**	**−1.55**	−1.45	−0.98
hcp	−1.88	**−1.82**	−1.34	−1.52	−1.45	−0.94

Table 2
Adsorption energies (in eV) calculated using PBE/PAW and RPBE/PAW for CO adsorption on Ag(111) for different CO_{ad} coverages. The labels T, fcc, hcp, and B denote adsorption in on-top, hollow-fcc, hollow-hcp, and bridge sites, respectively. Bold values denote the preferential adsorption site in each case.

	PBE/PAW			RPBE/PAW		
Θ_{CO}	1/9	1/3	2/3	1/9	1/3	2/3
T	−0.22	−0.20	**−0.07**	**0.01**	0.03	**0.19**
B	−0.26	−0.21	−0.01	0.05	**0.00**	0.20
fcc	**−0.28**	−0.22	0.06	0.22	0.03	0.21
hcp	−0.27	**−0.23**	0.07	0.22	0.01	0.20

bulk. The adsorption energies obtained for CO adsorption on different sites of the Ag_{1L}/Pt(111) surface, calculated using PBE/PAW and RPBE/PAW, are collected in Table 4. These calculations elucidate the influence of a Pt bulk underneath a Ag monolayer compared with a pure Ag bulk. Again CO adsorption energies are extremely low and those obtained with RPBE are smaller than those obtained using PBE (by 0.2 to 0.4 eV). Using PBE yields similar trends for this system as for the Ag(111) surface, and also the differences between different adsorption energies are of similar magnitude (few tens of meV). Using RPBE, in contrast the trends are different, since the CO molecule is stabilized in on-top sites (smaller positive values) at any coverage. Interestingly, the adsorption energies are of similar magnitude as obtained for adsorption on Ag(111). Apparently, the vertical ligand effects, which according to the simple concept of constant bond order should be destabilizing for CO adsorption on Ag/Pt(111), and strain effects, which for compressive strain should also be destabilizing, do not seem to matter. This agrees with previous findings that for monolayer structures of Pd/Au(111) [72] and Pt/Au(111) [71] systems simple arguments based on ligand and strain effects fail to fully describe the observed trends in the adsorption energy.

Similar to the previous section, we also calculated adsorption energies for CO adsorption at defect sites in the Ag_{1L}/Pt(111) surface. In general, we proceed as described for CO/$Ag_{2/3L}$/Ag(111) in the previous section, but now for a Ag monolayer covered Pt(111) surface. This results in close-packed double rows of Ag surface atoms along the <010> direction, separated by a missing row of Ag atoms. Hence, in these areas atoms of the underlying Pt(111) substrate would be accessible. Following the terminology introduced above, we denote the surface as $Ag_{2/3L}$/Pt(111).

Using PBE, we find the CO molecule to preferentially adsorb in on-top Ag sites at the upper level of the step edge with adsorption energies around −0.50 eV, again followed by adsorption in bridge sites with values in the range of −0.45 to −0.48 eV. CO adsorption at the lower level of the step edge, which in this case would reflect adsorption on Pt atoms, was not considered. Using RPBE, adsorption in on-top sites is also preferred with adsorption energies in the range of −0.24 to −0.26 eV, followed by adsorption in bridge sites (−0.15 eV to −0.19 eV). If the relaxation is started at hollow sites, the molecule moves towards on-top or bridge sites, similarly as for the $Ag_{2/3L}$/Ag(111) system.

Neither PBE nor RPBE functionals showed any significant difference in adsorption energies between the Ag_{1L}/Ag(111) surface and the Ag_{1L}/Pt(111) surface (see above), indicating that there is no distinct influence of the Pt bulk compared with a Ag bulk (both with their respective bulk spacing) on CO adsorption on ideal Ag sites on a Ag surface layer. This clearly changes when going to adsorption on Ag defect sites. In this case, CO adsorption on the upper terrace step sites on the $Ag_{2/3L}$/Pt(111) surface is significantly stabilized, by ~100 meV, compared with CO adsorption on the comparable step sites of the $Ag_{2/3L}$/Ag(111) surface. This difference, which is obtained for both functionals, clearly indicates a stabilizing influence of the Pt bulk compared with the Ag bulk, and hence the presence of vertical ligand effects when going to Ag defect sites.

3.2.4. The CO/Pt_xAg_{1-x}/Pt(111) system

Adsorption energies for CO adsorption on different Pt ensembles (monomers, dimers, compact trimers) in the surface layer were calculated for adsorption in on-top, bridge and threefold hollow sites (fcc and hcp sites) at a fixed CO_{ad} coverage of $\theta_{CO} = 1/9$ on surfaces with

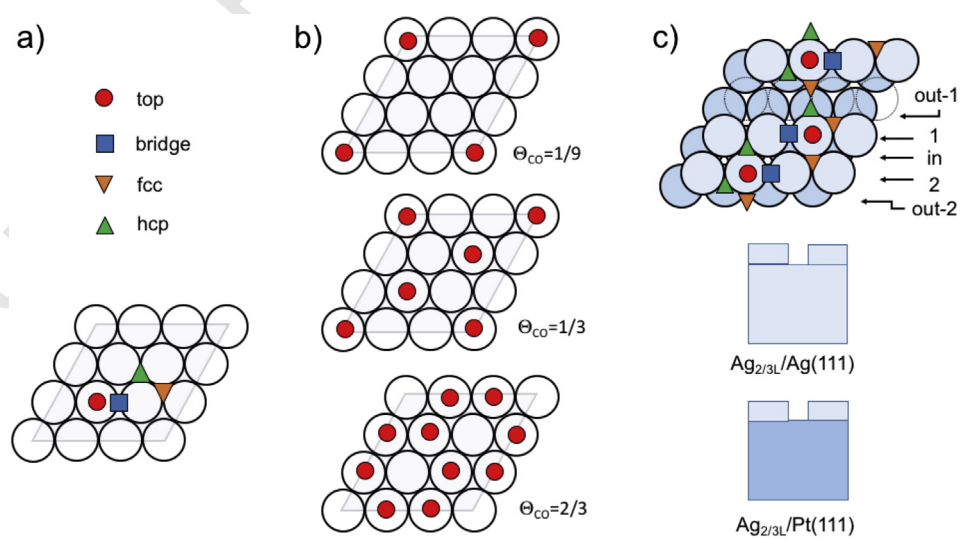

Fig. 9. Schematic presentation of the CO adsorption sites in a (3 × 3) unit cell. a) Notation for CO adsorption sites on a fcc(111) surface, b) distribution of adsorbed molecules on Pt(111) and Ag(111) at different coverages ($\theta_{CO} = 1/9$, 1/3 and 2/3 ML) shown for on-top sites, adsorption on the other sites follows a similar distribution. c) Adsorption sites investigated for CO adsorbed on Ag defect sites on the $Ag_{2/3L}$/Ag(111) and $Ag_{2/3L}$/Pt(111) defect structures ($\theta_{CO} = 1/9$ ML). These structures are obtained by removing a row of Ag atoms of the surface layer (missing atoms are denoted by dashed circles). Adsorption is considered at the upper level of the step edge as indicated in the cross sectional views of the surface.

Please cite this article as: K.M. Schüttler, et al., Interaction of CO with PtxAg1−x/Pt(111) surface alloys: More than dilution by Ag atoms, Surf. Sci. (2015), http://dx.doi.org/10.1016/j.susc.2015.12.022

Table 3
Adsorption energies (in eV) calculated using PBE/PAW and RPBE/PAW for CO adsorption on Ag defect sites on the $Ag_{2/3L}$/Ag(111) and $Ag_{2/3L}$/Pt(111) systems, considering different sites at the upper level of a step edge (see Fig. 9). The labels T, fcc, hcp, B denote adsorption in on-top, hollow-fcc, hollow-hcp and bridge sites, respectively. Bold values denote the preferential adsorption site in each case. The CO_{ad} coverage is 1/9. In each case we report the initial site before relaxation (as described in Fig. 9) and the final adsorption site. If the relaxation is started at hollow sites the CO molecule moves towards on-top or bridge sites.

Site		PBE/PAW		RPBE/PAW	
Initial	After relaxation	$Ag_{2/3L}$/Ag(111)	$Ag_{2/3L}$/Pt(111)	$Ag_{2/3L}$/Ag(111)	$Ag_{2/3L}$/Pt(111)
T-1	T (tilted-in)	−0.36	**−0.50**	−0.15	−0.25
T-2	T (tilted-in)	−0.38	−0.49	−0.16	−0.24
B-1	B (tilted-in)	−0.35	−0.46	−0.07	−0.17
B-2	B (tilted-in)	−0.36	−0.46	−0.08	−0.17
fcc-in	B (tilted-in)	−0.33	−0.45	−0.08	−0.16
fcc-out-1	B (tilted-out)	−0.37	−0.48	−0.09	−0.19
fcc-out-2	T (tilted-out)	**−0.41**	−0.49	**−0.19**	−0.25
hcp-in	B (tilted-in)	−0.34	−0.46	−0.06	−0.15
hcp-out-1	T (tilted-out)	−0.38	−0.50	−0.16	**−0.26**
hcp-out-2	B (tilted-out)	−0.38	−0.48	−0.10	−0.18

one Pt ensemble per (3 × 3) unit cell. Table 5 shows the resulting adsorption energies, calculated using PBE or RPBE. The trends are identical for both functionals, and therefore only those for PBE are given in Fig. 10. For comparison, also values calculated for Pd based ensembles are shown [22] Fig. 10a shows adsorption energies for the different adsorption sites possible on the respective ensembles. The development of the adsorption energies for adsorption in on-top sites is illustrated by dashed lines both for Pt and Pd based surfaces. Fig. 10b only shows the most stable adsorption sites in each case; in this case the trend of these adsorption energies is illustrated by dashed lines. For Pt(111) the dashed line ends between the value calculated for on-top and fcc adsorption sites in order to illustrate the "CO/Pt(111) puzzle", i.e., the erroneous prediction of the most stable adsorption site by DFT calculations. These ensembles represent CO adsorption on Pt sites in the surface alloys which are perturbed by Ag neighbors, where the perturbation includes both electronic effects (lateral ligand effects) and geometric compression due to the larger size of the Ag surface atoms (strain effects). Again the CO adsorption energies obtained with RPBE are in general smaller than those obtained using PBE, but the trends of the results are similar, and the site preference for adsorption is independent of the choice of the functional. Independent of the Pt ensemble size, the CO molecule always adsorbs preferentially in on-top sites of the Pt_1, Pt_2, and Pt_3 ensembles of the Pt_xAg_{1-x}/Pt(111) surface alloys, with decreasing adsorption energy when going to larger ensembles, from Pt_1 to Pt_3 and finally to Pt(111) (Fig. 10). Considering our previous assumption that small ensembles are also a reasonable model for the description of CO adsorption on mixed surfaces with higher Pt contents it is important to note that the differences in adsorption energy between on-top adsorption on Pt_3 trimers and on Pt(111) are rather small. This confirms the validity of our above assumption that adsorption on a Pt atom in a Pt_3 trimer is already a reasonable model also for adsorption in on-top sites of larger ensembles. The same holds true for the other sites.

In order to predict the adsorption strength of the Pt_xAg_{1-x}/Pt(111) surface alloys as a function of their composition within the d-band model [12,73], we furthermore determined the local density of states (LDOS) for Pt atoms in the topmost layer for the Pt_1, Pt_2, and Pt_3 ensembles (Pt coverages 1/9, 2/9 and 3/9 respectively). Fig. 11 shows the local DOS projected onto the Pt 5d states for the pure Pt(111) surface and for the three corresponding surface alloys as calculated using PBE. For the pure Pt(111) surface the center of the d-band is located at −2.07 eV. For Pt_xAg_{1-x}/Pt(111) surface alloys with low Pt concentrations (viz., Pt_1Ag_8 to Pt_3Ag_6), alloying with Ag leads to an up-shift of the center of the d-band at the Pt atoms in the uppermost layer. For Pt_1Ag_8, the center of the d-band at the Pt atom is located at −1.49 eV. Increasing the size of the Pt ensembles in the overlayer brings the center of the d-band closer to that of pure Pt(111), to −1.65 eV for Pt_2Ag_7 and to −1.72 eV for Pt_3Ag_6. This trend in d-band energy shows that the ligand effect due to the interaction with the more inert Ag atoms overcompensates the compressive strain effect due to the larger size of the Ag atoms. Hence, according to the d-band model [12,73], the Pt surface atoms are more strongly binding in all of the mixed configuration than Pt surface atoms in pure Pt(111), since in each of these cases the center of the d-band is closer to the Fermi energy. The same trends in the behavior of the d-band center were found when using RPBE/PAW. Here, the center of the d-band was located at −2.00 eV for Pt(111), while for surface alloys with Pt_1, Pt_2 and Pt_3 ensembles, the values are −1.48 eV, −1.63 eV and −1.69 eV, respectively.

In most cases, adsorption energies obtained using RPBE are 0.3–0.4 eV smaller compared with PBE. Furthermore, although both functionals provide different pictures (adsorption site preferences) for CO adsorption either on Pt(111) or on Ag(111), both predict similar trends for the case of the bimetallic Pt_xAg_{1-x}/Pt(111) surface alloys, indicating that either of these two functionals could be used to systematically study CO adsorption on these surface alloys. Finally, looking at the maximum CO adsorption energies in the different systems for a CO coverage of $\Theta_{CO} = 1/9$, we have the following trends (using PBE, independent of the preferred sites): −0.28 eV for Ag(111), −0.28 eV for Ag_{1L}/Pt(111), −0.41 eV for $Ag_{2/3L}$/Ag(111), −0.51 eV for $Ag_{2/3L}$/Pt(111), −1.91 eV for Pt(111), and −2.06 eV for Pt_1Ag_8/Pt(111). A similar trend is obtained when we use RPBE. Our calculated adsorption energy values agree well with trends reported for the CO desorption temperatures: 50 K for Ag(111) [51], 80–90 K for step sites on a Ag(111) surface [52], and

Table 4
Adsorption energies (in eV) calculated using PBE/PAW and RPBE/PAW functionals for CO adsorption on Ag_{1L}/Pt(111) for different CO_{ad} coverages. The labels T, fcc, hcp, and B denote adsorption in on-top, hollow-fcc, hollow-hcp, and bridge sites, respectively. Bold values denote the preferential adsorption site in each case.

	PBE/PAW			RPBE/PAW		
Θ_{CO}	1/9	1/3	2/3	1/9	1/3	2/3
T	−0.27	−0.22	**−0.02**	**0.00**	**0.05**	**0.30**
B	−0.26	−0.21	0.07	0.07	0.12	0.43
fcc	**−0.28**	**−0.23**	0.14	0.07	0.12	0.50
hcp	−0.27	−0.21	0.14	0.08	0.14	0.50

Table 5
Adsorption energies (in eV) calculated using PBE/PAW and RPBE/PAW for CO adsorption on Pt_xAg_{1-x}/Pt(111) surface alloys considering Pt_1, Pt_2, and Pt_3 ensembles. The labels T, fcc, hcp, B denote CO adsorption in on-top, hollow-fcc, hollow-hcp and bridge sites, respectively. Bold values denote the preferential adsorption site in each case. The CO_{ad} coverage is 1/9.

	Site	PBE/PAW	RPBE/PAW
Pt_1	T	**−2.06**	**−1.74**
Pt_2	T	**−1.98**	**−1.67**
	B	−1.95	−1.58
Pt_3	T	**−1.96**	**−1.66**
	fcc	−1.94	−1.56
	hcp	−1.92	−1.54

Please cite this article as: K.M. Schüttler, et al., Interaction of CO with PtxAg1−x/Pt(111) surface alloys: More than dilution by Ag atoms, Surf. Sci. (2015), http://dx.doi.org/10.1016/j.susc.2015.12.022

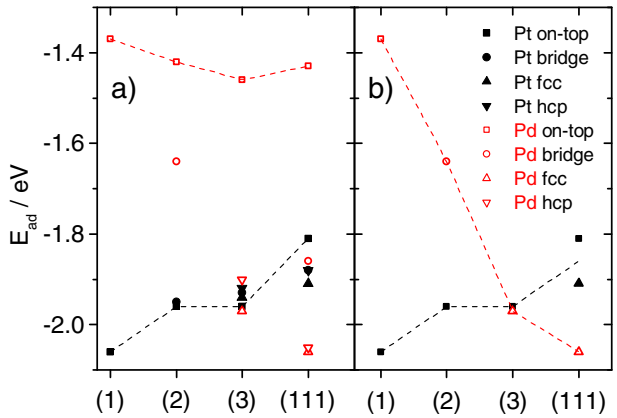

Fig. 10. a) Trend of the CO adsorption energy (1 CO per Pt ensemble) on different sites on Pt_1Ag_8/Pt(111), Pt_2Ag_7/Pt(111) and Pt_3Ag_6/Pt(111), and for comparison on Pt(111) (black filled symbols). Numbers on the x axis indicate the ensemble size: (1) for monomers; (2) for dimers, (3) for compact trimers and (111) for a (111)-like surface. b) Trend of the CO adsorption energy with increasing Pt_n ensemble site on the above systems using the most stable adsorption site for each ensemble, and for comparison on Pt(111) (for Pt(111) both on-top and threefold hollow site adsorption are included because of the "CO/Pt(111) puzzle"). Values for adsorption on similar sites on Pd_xAg_{1-x}/Pd(111) (red empty symbols) illustrate the difference between Pt(111)- and Pd(111)-based surface alloys. Results were obtained using PBE/PAW, dashed lines are meant as guide for the eye. (For interpretation of the references to color in this figure legend, the reader is referred to the web version of this article.)

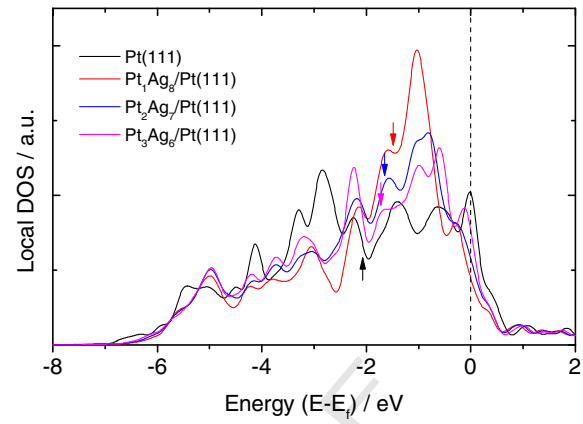

Fig. 11. Local density of d-states calculated by projection of the 5d wave functions onto the atomic orbitals at a Pt on-top-site. Four cases are presented: the pure Pt(111) surface and PtAg surface alloys containing Pt_1, Pt_2 and Pt_3 ensembles. All energy values are referred to the Fermi energy. Arrow pointing up denotes the position of the d-band center for the Pt(111) surface and arrows pointing down denote the positions of the d-band center for the surface alloys. Results were obtained using PBE/PAW.

120 K for desorption from island edges of a Pt(111) surface covered by monolayer Ag islands [74]. The latter value is quite similar to the 140 K detected in the present study (see Section 3.1.2).

3.2.5. The CO/Pt_xAg_{1-x}/Ag_{nL}/Pt(111) system

Finally, we investigated the effect of Ag in subsurface layers by substituting one (Table 6) or two (Table 7) layers of Pt directly under the mixed surface layer by Ag layer(s). Interestingly, replacement of one layer of Pt directly underneath the alloyed layer by Ag leads for all ensembles to a pronounced weakening of the Pt–CO bonding. The adsorption energy for the most strongly bound CO molecule adsorbed in the Pt_1Ag_8 ensemble is reduced by almost ~0.55 eV, so that the adsorption energy is even ~0.4 eV lower than for Pt(111). For the Pt_2Ag_7 and Pt_3Ag_6 ensemble, the CO adsorption energy is reduced by ~0.6–0.7 eV at the on-top sites, but only by ~0.4–0.5 eV at the bridge or hollow sites, thus changing the preferred adsorption site from on-top to bridge at Pt_2 and from on-top to hollow-hcp at Pt_3. This destabilization is in contrast to expectations based on bond order arguments [75]. According to that model one would expect a stronger Pt–CO bond in the CO/Pt_xAg_{1-x}/Ag_{nL}/Pt(111) system due to the weaker Pt–Ag bond to the second layer as compared with the Pt–Pt bond in CO/Pt_xAg_{1-x}/Pt(111). In contrast to the stabilizing vertical ligand effects, strain effects should not play a role, since the surface layer has a similar structure in both configurations. Obviously, these simple ideas do not agree with the predictions from theory.

Comparable effects are observed when replacing a second Pt layer by Ag; the CO adsorption energies become slightly higher again, but are still ~0.3 eV lower than for Pt(111) and the site preference is changed in the same way as obtained for a single Ag sub-layer. Hence, also in this case the trend is opposite from expectations based on the constant bond order concept. On the other hand, it appears to be consistent that making the Ag slab thicker reverts the changes introduced by replacing the 2nd Pt layer by a Ag layer.

In order to see whether the destabilization of the Pt–CO bond induced by the Ag sub-layer is reflected also by a down-shift of the d-band center, as expected from the d-band model, we determined the local density of states (LDOS) at the Pt atom in the topmost layer (Pt coverage 1/9). The introduction of one or two Ag sub-layers shifts the center of the d-band at the Pt atom in the mixed surface from −1.49 eV to −1.51 eV and −1.56 eV, respectively, equivalent to a small down-shift in energy, however, the shape of the d-band is altered significantly. This shows that the significant change in the CO adsorption energy upon introduction of the Ag sub-layers cannot be explained based on the change of the d-band centers alone. (Note that the center of the d-band on the Pt atom in the Pt_1Ag_8/Pt(111) system is located at −1.49 eV, i.e., significantly closer to the Fermi energy than the d-band center of the pure Pt(111) at −2.07 eV, as already mentioned in Section 3.2.4).

Hence, the d-band model also gives no explanation for the strong reduction in the Pt–CO binding upon the introduction of a Ag second layer. Recently, it was shown that in the so-called near-surface alloys with a layer of a foreign metal as the second layer, simple arguments based on the d-band model are not adequate. Rather, scaling relations with respect to the valence configuration should be invoked [76], but it has also been proposed that the shape of the d-band with its upper edge location should be considered [77].

In total, these results show that the (hypothetical) replacement of one or two Pt layers below the surface by Ag does not stabilize the CO adsorption on the Pt atoms of the surface alloy but instead weakens it. Interestingly, similar trends had been obtained in calculations for CO adsorption on Pd_xAg_{1-x}/Pd(111) surface alloys [22]. In the latter case, this was supported also by experimental evidence, by the appearance of a CO desorption peak from Pd_1 monomers at lower temperatures for very high Ag contents, where incorporation of Ag atoms in the second layer was likely [21]. In the present case, we do not have any experimental indications for a weakening of the Pt–CO bond by Ag underneath, most likely since diffusion of Ag into deeper layer is much less probable than for Pd_xAg_{1-x}/Pd(111) surface alloys.

4. Discussion

In the following sections, we will discuss in more detail some specific aspects of the results presented in the previous section, which are of general relevance for the understanding of adsorption and specifically of CO adsorption on bimetallic surfaces. We will first focus on modifications of the metal–CO bond for CO adsorbed on bimetallic Pt_xAg_{1-x}/Pt(111) surfaces compared with CO adsorption on the respective bulk substrates (Section 4.1). This will include modifications of the Pt–CO bond induced by neighboring Ag ligand atoms (Section 4.1.1), followed by modifications in the Ag–CO bond induced by neighboring Pt atoms (Section 4.1.2). Secondly, we will systematically compare the present results with previous findings on CO adsorption on the closely related Pt_xAu_{1-x}/Pt(111) surface alloy as Pt-based system and the Pd_xAg_{1-x}/Pd(111) as well as Pd_xAu_{1-x}/Pd(111) surface alloys as Pd-based systems. In the discussion,

Please cite this article as: K.M. Schüttler, et al., Interaction of CO with PtxAg1−x/Pt(111) surface alloys: More than dilution by Ag atoms, Surf. Sci. (2015), http://dx.doi.org/10.1016/j.susc.2015.12.022

Table 6
Adsorption energies (in eV) calculated using PBE/PAW and RPBE/PAW for CO adsorption on a $Pt_xAg_{1-x}/Ag_{1L}/Pt(111)$ system considering Pt_1, Pt_2, and Pt_3 ensembles. The labels T, fcc, hcp, B denote adsorption in on-top, hollow-fcc, hollow-hcp and bridge sites, respectively. Bold values denote the preferential adsorption site in each case. The CO_{ad} coverage is 1/9.

	Site	PBE/PAW	RPBE/PAW
Pt_1	T	**−1.50**	**−1.19**
Pt_2	T	−1.34	−1.02
	B	**−1.53**	**−1.14**
Pt_3	T	−1.28	−0.98
	fcc	−1.48	−1.07
	hcp	**−1.52**	**−1.11**

we will focus on experimental/theoretical data obtained for small CO exposure, at low CO_{ad} coverages, where repulsive CO_{ad}–CO_{ad} interactions (as well as dynamic dipole coupling [58] in IR experiments) can be neglected under these conditions. Therefore, they illustrate more directly the influence of increasing Ag content in the $Pt_xAg_{1-x}/Pt(111)$ surface alloy on the CO adsorption properties compared with unmodified Pt(111), and the same holds true also for the other systems.

4.1. CO adsorption on modified sites in $Pt_xAg_{1-x}/Pt(111)$ surface alloys

Modification of the adsorption properties of specific surface atoms or ensembles of surface atoms in a surface alloy can be introduced by different type neighbors and/or by replacement of underlying substrate atoms by different type species. In both cases electronic ligand and strain effects apply, while ensemble effects are essentially absent for CO adsorption on $Pt_xAg_{1-x}/Pt(111)$ surface alloys. In all cases, adsorption in on-top Pt sites is most stable, and for adsorption on Ag sites the differences are mostly below the experimental detection limit. The influence of replacing sub-surface Pt atoms by Ag, and the unexpected destabilization of the Pt–CO bond resulting from sub-surface Ag atoms was already discussed in detail in Section 3.2.5 and shall not be repeated here. For CO adsorption on Ag surface atoms the influence of Ag sub-surface atoms was not calculated, but considering the little difference between adsorption on Ag surface atoms on Ag(111) and on Ag_{1L}/Pt(111) we expect negligible effects.

4.1.1. CO adsorption on Ag modified Pt sites

In the simple model of constant bond order, which had been put forward to describe the influence of electronic ligand effects on the adsorption on bimetallic surfaces [75], one would expect that the presence of Ag in the surface layer should stabilize CO adsorption on adjacent Pt sites: since the center of the d-band of Ag(111) is located at much lower energy compared with Pt(111), the interaction of a Ag atom with a Pt atom should be much weaker compared with the Pt–Pt interaction, leading to a stronger binding of a CO molecule to a Pt surface atom surrounded by Ag atoms than to a Pt atom in a Pt(111) surface. On the other hand, strain effects in the above mentioned configuration should result in a destabilization of the Pt–CO bond due to compressive strain in the pseudomorphic alloy layer caused by the insertion of the larger Ag atom (lattice constant 4.08 vs. 3.92 Å, resulting lattice mismatch +4.1%) [11,12,73].

For the present system, the stabilizing ligand effect seems to clearly dominate over the destabilizing strain effect. A stabilization of CO adsorption had been observed already at the lowest Ag content of 10%, where at low CO_{ad} coverage the whole desorption peak is shifted by 15 K to higher temperature. Simultaneously, the corresponding IR band shifts from 2090 to 2079 resp. 2072 cm^{-1}, reflecting a stronger $2\pi^*$ back donation. At 20% Ag, this effect becomes more pronounced: the TPD peak is shifted by another 15 K to higher temperature, along with a further shift of the corresponding IR bands to 2068 resp. 2060 cm^{-1}. The stabilization is also confirmed by the DFT calculations, which show a much stronger binding of CO on the Pt atom of a Pt_1Ag_8 ensemble ($CO/Pt_1Ag_8/Pt(111)$) compared with adsorption on Pt(111) at low CO coverage. The origin of this stabilizing effect is an upshift of the d-band center on the Pt surface atoms as a sum of ligand and strain effects, as shown in DFT calculations for all three adsorption complexes investigated.

Most obvious is the stabilization of the adsorbed CO in the high temperature desorption peak in the CO TPD spectra. Such kind of peak ($T_{max} \approx 550$ K) was already reported by Strüber and Küppers for CO desorption from Ag films on Pt(111) annealed at 760 K [31]. They ascribed it to CO desorption from "Pt clusters embedded in Ag islands". Based on the amount of Ag deposition (0.8 ML) and on the annealing pretreatment, these surfaces are very close to the present surface alloys with high Ag content [28], and therefore the nature and origin of the high-temperature desorption peak should be identical in both cases. Not resolved, however, is the exact nature of the adsorption site responsible for this desorption peak. Different Pt_n ensembles were found to stabilize the adsorption of CO. On the other hand, the calculations revealed that sub-surface Ag results in a destabilization of adsorbed CO (see Section 3.2.5), indicating that this cannot be responsible for the formation of the high temperature CO desorption peak.

The experimental observation that CO molecules adsorbed in this site do not interact with other adsorbed CO molecules at saturation coverage suggests small Pt ensembles such as Pt_1 monomers or Pt_2 dimers surrounded by Ag surface atoms as adsorption site. In that case, diffusional transport and interactions with CO adsorbed outside the Pt ensemble are inhibited. Adsorption on Pt_1 monomers could properly explain the observed stabilization of adsorbed CO. Considering the strong tendency for phase separation in $Pt_xAg_{1-x}/Pt(111)$ surface alloys, however, we doubt that such sites are already formed at 50% of Ag in sufficient amounts. STM images show significant amounts of isolated Pt monomers only at the highest concentration investigated, at 95% Ag [27]. Including also Pt_2 dimers increases the number of available Pt sites, but it is still far too low to account for the intensity in the high temperature desorption peak over the entire composition range. Based on the combination of STM data and calculations we expect Pt atoms surrounded by 6 or 5, and possibly also by 4 Ag surface atoms, as they are present in small Pt ensembles (monomers, dimers) but also at edge/corner sites of narrow Pt structures in larger ensembles, to be responsible for the stabilized CO_{ad} species desorbing in the high-temperature peak. Such structures can be observed in STM images at above 40–50% Ag. Desorption of the last CO molecule adsorbed on such a site should behave almost like CO on a Pt monomer (see Section 3.2.4).

Interestingly, after CO adsorption at low temperature, the IR band corresponding to these sites only has a very low intensity, independent of the CO_{ad} coverage. After stepwise annealing of these surface alloys to successively desorb CO_{ad}, its intensity increases, reaching its maximum value after annealing to 500 K, when all CO_{ad} desorbing in the main desorption peak has been removed. The explanation for this experimental observation depends on the CO_{ad} coverage. After small CO exposure at low temperature, the fraction of these small Pt ensembles populated with CO simply is too low to be able to detect the corresponding IR-band, since they are only populated statistically by CO molecules impinging at the right Pt ensemble; subsequent surface diffusion to these

Table 7
Adsorption energies (in eV) calculated using PBE/PAW and RPBE/PAW for CO adsorption on a $Pt_xAg_{1-x}/Ag_{2L}/Pt(111)$ system considering Pt_1, Pt_2, and Pt_3 ensembles. The labels T, fcc, hcp, B denote adsorption in on-top, hollow-fcc, hollow-hcp and bridge sites, respectively. Bold values denote the preferential adsorption site in each case. The CO_{ad} coverage is 1/9.

	Site	PBE/PAW	RPBE/PAW
Pt_1	T	**−1.63**	**−1.31**
Pt_2	T	−1.49	−1.18
	B	**−1.69**	**−1.29**
Pt_3	T	−1.40	−1.09
	fcc	−1.65	−1.23
	hcp	**−1.70**	**−1.28**

Please cite this article as: K.M. Schüttler, et al., Interaction of CO with PtxAg1−x/Pt(111) surface alloys: More than dilution by Ag atoms, Surf. Sci. (2015), http://dx.doi.org/10.1016/j.susc.2015.12.022

ensembles is inhibited, as indicated by the simultaneous growth of main- and high temperature desorption feature at low CO_{ad} coverage and also by the low adsorption energy of CO on Ag sites separating the Pt ensembles.

After larger CO exposures, up to saturation of the surface with CO_{ad}, all ensembles are populated. In that case, however, ensembles containing more than one Pt surface atom will contain more than one CO_{ad} molecule, up to one CO molecule per Pt atom. This leads to a shift of the vibrational frequency to higher wavenumbers due to repulsive interactions between these CO molecules on the one hand and to an intensity loss due to depolarization on the other hand. When successively heating a surface saturated with CO_{ad} at low temperature, most CO molecules adsorbed on larger ensembles will desorb in the main desorption feature, so that after heating to 500 K all of these ensembles are still populated, but with only 'non-interacting' CO_{ad} species, e.g., one CO_{ad} molecule in the case of Pt dimers. In this case, frequency shifts and depolarization effects are absent, and the corresponding IR band reaches its full intensity.

In summary, we attribute desorption in the high-temperature peak to desorption of non-interacting CO_{ad} molecules from Pt sites, where the corresponding Pt atom is surrounded by at least 4 Ag surface atoms. This assignment is compatible with all experimental findings and it is also in good agreement with the observed stabilization of CO_{ad} according to DFT calculations. Finally, the appearance of these sites at ca. 50% Ag surface content agrees with results of the STM measurements.

4.1.2. CO adsorption on Pt modified Ag sites

For all Pt_xAg_{1-x}/Pt(111) surface alloys, a small desorption feature was observed directly after starting the heating ramp (desorption maximum 130–140 K). This was never observed before Ag deposition and is therefore assigned to desorption from Ag sites. Its intensity did not change very much with increasing Ag content and remained very small ($\theta_{CO} < 0.01$ ML) for all surface alloys studied. Therefore, we assigned it to CO desorption from Ag atoms located at steps or other defects of the surface alloy layer. For bulk Ag surfaces, CO desorption was observed at ~50 K for a flat Ag(111) surface [51] and at 80–90 K from the step sites of a Ag(221) surface [52]. The additional stabilization compared with bulk Ag surfaces observed for the surface alloys must be due to an electronic effect induced by the Pt(111) substrate. A similar stabilization was reported by Rodriguez et al. for CO adsorption on Ag-decorated Pt(111) surfaces [74]. After deposition of sub-monolayer Ag amounts on a Pt(111) surface at low temperature (90 K), they observed CO adsorbed on Ag sites up to 120 K, and identified these as Ag defect sites with an additional stabilization by the Pt bulk [74].

DFT calculations performed for CO adsorbed on a Ag surface atom/Ag site surprisingly did not show any significant difference between a pseudomorphic Ag monolayer on Pt(111) and on Ag(111) as substrate, indicating that interaction with the Pt(111) bulk surface does neither stabilize nor destabilize CO adsorption on the Ag surface layer. This changes, however, when going to defect sites. For CO adsorbed on a Ag site directly at the edge of a Ag step the underlying Pt(111) substrate was found to clearly stabilize the Ag–CO bond compared with adsorption on a similar site on Ag(111) by about 100 meV at low CO_{ad} coverage. The physical origin of the different substrate effects in these two cases, in the Ag edge configuration and in the closed Ag overlayer, remains unclear in the moment. It should also be noted that if steps are considered, CO adsorption occurs preferentially in on-top sites at the upper level step edge, both for the $Ag_{2/3L}$/Ag(111) and for the $Ag_{2/3L}$/Pt(111) surfaces.

Due to the low coverage of these CO_{ad} species we could not detect an IR band which could be correlated with the low temperature desorption feature. Such bands were reported previously, however, for surfaces with a high enough concentration of Ag defect sites, which were created e.g., by Ag deposition at low temperatures (Ag/Ag film [78], Ag/Pt(111) [74]). For these surfaces, bands around 2150 cm^{-1} were associated with CO_{ad} species on these Ag defect sites, both for Ag/Ag film and for Ag/Pt(111). This is very close to CO adsorption on Ag(111) which shows a band at 2153 cm^{-1} [51]. Hence, both experiment and calculations clearly demonstrate a stabilizing effect of a Pt(111) bulk on CO adsorption on Ag defect sites, in agreement with previous findings [74], but there was no significant change in the C–O vibrational properties. Q8

4.2. Comparison with CO adsorption on related bimetallic surfaces

Finally, we would like to compare the results obtained from the Pt_xAg_{1-x}/Pt(111) system investigated in this study with CO adsorption studies on surface alloys of a similar type, including Pt_xAu_{1-x}/Pt(111) [23], Pd_xAg_{1-x}/Pd(111) [20–22] and Pd_xAu_{1-x}/Pd(111) [19,79].

4.2.1. Distribution of surface atoms

First of all, these different surface alloy systems, though consisting of rather comparable metals, exhibit very different structural characteristics. Pt_xAu_{1-x}/Pt(111) surface alloys also exhibit a significant tendency for phase separation, but it is much less pronounced than in the present Pt_xAg_{1-x}/Pt(111) system [26]. Similar to the present case, diffusion of the coinage metal (Au) into sub-surface regions was negligible for coverages up to almost monolayer coverage. Pd_xAg_{1-x}/Pd(111) surface alloys show a disperse distribution of surface atoms at lower Ag content, while at higher Ag content there is a slight tendency to phase separated clustering [25]. Pd_xAu_{1-x}/Pd(111) surface alloys finally show an almost statistical distribution of the surface atoms [24]. In both of the latter cases, some loss of the coinage metal into the near surface regions of the Pd bulk can be observed upon annealing of samples with higher Ag, Au contents at the temperature necessary for surface alloy formation. Hence, for the Pd based systems effects caused by the presence of Ag or Au atoms in the second layer are more likely for rather high Ag or Au contents than for the respective Pt analogs.

4.2.2. Ensemble effects

It is well known, that in Pd-based systems, including Pd(111), the adsorption energetics are dominated by the geometric ensemble effect due to the preference of CO for adsorption in a threefold hollow sites on Pd_3 trimers [19–22,79–81]. In Pt-based systems, however, on-top adsorption is favored, and bridge-bonded adsorption occurs only at higher CO coverage, if at all [20,21,23,46,53]. Therefore, ensemble effects should not play a big role and can easily be excluded by working at low CO coverage, where the adsorption behavior is determined by electronic ligand and strain effects.

The difference between Pd-based and Pt-based surface alloys is illustrated by the different trends of the CO adsorption energies for the different ensembles on Pd_xAg_{1-x}/Pd(111) and on Pt_xAg_{1-x}/Pt(111) surface alloys (Fig. 10b). For Pd_xAg_{1-x}/Pd(111) this shows a pronounced stabilization when going from CO adsorption on a Pd_1 monomer via a Pd_2 dimer and a Pd_3 trimer, always using the most stable adsorption site, to finally adsorption on Pd(111), while for a similar sequence on the Pt-based system we find a destabilization. This marked difference is mainly caused by the pronounced stabilization of the Pd–CO bond when adsorbing on higher coordination sites, which requires Pd_2 dimers (bridge sites) and Pd_3 compact trimers (hollow sites) at minimum or larger ensembles; it is much less pronounced when keeping the adsorption site. In contrast, for the Pt_xAg_{1-x}/Pt(111) surface alloy, where adsorption is always most stable in the on-top site (except for Pt(111) where due to the "CO/Pt(111) puzzle" adsorption on the hollow sites appears as more stable in the DFT calculations), the combined ligand + strain effects dominate the trend of the CO adsorption energy and result in a destabilization with increasing Pt_n ensemble size (Fig. 10b).

In combination with the distinct differences in the distribution of surface atoms, the different ensemble effects in the 2 types of surface alloys lead to considerable differences in the CO adsorption behavior. For Pt-based surface alloys, the growth of the Pt ensembles, from Pt_1 monomers to Pt_2 dimers, compact Pt_3 trimers and bigger ensembles, does not allow the occupation of more stable adsorption sites. Actually, increasing

Please cite this article as: K.M. Schüttler, et al., Interaction of CO with PtxAg1−x/Pt(111) surface alloys: More than dilution by Ag atoms, Surf. Sci. (2015), http://dx.doi.org/10.1016/j.susc.2015.12.022

ensemble size leads to a destabilization of the Pt–CO interaction. This is different for the Pd-based surface alloys, where a transition to larger ensembles leads, in average, to a stabilization of the CO adlayer. The small size of the Pd ensembles at low Pd contents and their slow growth with increasing Pd surface, following the trend for a statistical distribution, result in a distinct stabilization of CO_{ad} with increasing Pd surface content.

For Pt_xAg_{1-x}/Pt(111), where an increasing size of the Pt ensemble results in a destabilization of the Pt–CO bond (with adsorption always in on-top sites), the observed effects (in the main desorption peak) are small, since already at low Pt surface contents rather large Pt ensembles prevail. A stabilization of the adsorbed CO appears only for CO adsorption on Pt surface atoms which are surrounded by at least 4, if not 5, Ag surface atoms (see Section 4.1.1). Desorption of non-interacting CO_{ad} molecules on these sites/ensembles, which are present in the lower CO_{ad} coverage regime, results in the distinct high temperature peak with its maximum at about 550 K. Finally, for Pt_xAu_{1-x}/Pt(111), where stabilization of the Pt–CO bond by lateral ligand effects and destabilization by strain effects seem to largely cancel out and where, like in the present case, ensemble effects are absent [23], there is hardly any change in the Pt–CO bond with increasing Pt surface content. Accordingly, there are no distinct changes in the CO TPD spectra with increasing Pt surface content except for an increase in desorption intensity.

4.2.3. Ligand and strain effects

As a third point we want to compare the role and size of (lateral) ligand effects and strain effects, which determine the changes in the metal–CO bond upon replacing adjacent surface atoms by the respective other species, e.g., Pt surface atoms around a central Pt surface atom by Ag atoms.

Alloying a Pt-group metal with a coinage metal of a larger size generally leads to two competing effects: compressive strain because of the addition of a larger atom and the weaker interaction of the Pt–group metal atom with the surrounding coinage metal atoms as compared with interaction with similar type surface atoms (lateral ligand effects). Based on the simple principle of constant bond order [75], weaker interactions with a neighboring metal atom should result in a stronger bond to the respective adsorbate. In the absence of changes in other contributions, in particular from strain effects, this should lead to a strengthening of the Pt–CO or Pd–CO bond. For the present case of Pt_xAg_{1-x}/Pt(111) surface alloys the stabilizing ligand effects seem to be dominant, at least for ensemble sizes up to Pt_3. For on-top adsorption the difference between CO adsorption on a Pt_1 monomer and on Pt(111) was calculated to be around 0.4 eV. This is in contrast to Pd_xAg_{1-x}/Pd(111) surface alloys, where the counteracting ligand and strain effects seem to cancel out. For the same adsorption site the resulting adsorption energies depend only little on the ensemble size. For on-top adsorption the difference between CO adsorption on a Pd_1 monomer and on Pd(111) was calculated to be around −0.06 eV, and for adsorption in on-top sites of larger Pd ensembles that difference was even smaller. For further details see ref. [22].

Moving to Pt_xAu_{1-x}/Pt(111) surface alloys, CO TPD measurements after small CO exposures did not show any significant shift of the peak temperature with Au content [23]. From that, the authors concluded that electronic ligand effects and strain effects seem to cancel out each other, and therefore do not modify the CO binding. Most interestingly, a continuous shift of the IR band due to on-top adsorption of CO on Pt sites to lower wavenumber was observed. This finding was explained by a change of the weight of the different contributions for CO adsorption to the Pt atoms of the PtAu/Pt(111) surface alloys with an increased contribution of the $2\pi^*$ back donation [23]. Calculations for CO adsorption on different ensemble structures confirmed the above trends, showing only a small destabilization for CO adsorption in an on-top site with increasing ensemble size, by about 0.1 eV, when going from CO adsorption on a Pt_1 monomer in $Pt_{0.33}Au_{0.67}$/Pt(111) via adsorption on a Pt atom with three Pt ligands in $Pt_{0.67}Au_{0.33}$/Pt(111) to adsorption on Pt(111) [82]. For CO adsorption on Pd_xAu_{1-x}/Pd(111) surface alloys, calculations revealed a very small stabilization by the combined ligand and strain effects with increasing ensemble size, e.g., from −0.71 eV for on-top adsorption on a Pd_1 monomer via −0.76 eV both on a Pd_2 dimer and a Pd_3 linear trimer to −0.98 eV on Pd(111), and similar results were obtained also for CO adsorption in bridge sites, where the adsorption energy increased from −0.87 eV on a Pd_2 dimer to −0.90 eV on a linear Pd_3 trimer [19,79]. Dominant effect in that system is the effective stabilization by ensemble effects, i.e., by a variation of the adsorption site, which causes an increase from −0.71 eV (Pd_1 monomer, on-top) via −0.87 eV (Pd_2 dimer, bridge site) to −1.11 eV (compact trimer, threefold hollow site). The trends in the experimental data were in excellent agreement with those derived from the calculations [19]. Overall, the results closely resemble the findings for CO adsorption on Pd_xAg_{1-x}/Pd(111) discussed above.

In total, the above results show that the combined (lateral) ligand and strain effects induced by Ag are stronger for Pt surface atoms/ensembles than for Pd surface atoms/ensembles on the respective substrates. Since (destabilizing) strain effects should be of comparable size for Pt_xAg_{1-x}/Pt(111) and Pd_xAg_{1-x}/Pd(111), considering the rather similar lattice constants of Pd (3.8898 Å) and Pt (3.9231 Å), respectively [42], this must be due to pronounced differences in the (stabilizing) ligand effects. In contrast, for the corresponding surface alloys with Au as second component the differences between the combined lateral ligand and strain effects are much less pronounced for both the Pd(111) and Pt(111)-based surface alloys. As a result, the stabilization of the Pt–CO bond induced by a neighborhood of Ag surface atoms in Pt_xAg_{1-x}/Pt(111) surface alloys, which is reflected by the formation of the high-temperature CO desorption peak, is a unique feature on a quantitative scale, while on a qualitative scale the stabilization agrees with findings for the other surface alloys discussed above.

These differences are reflected also by the respective shifts in the center of the d-band, which according to the d-band model are correlated with a strengthening (up-shift) or weakening (down-shift) of the metal–adsorbate bond. While for Pt_xAg_{1-x}/Pt(111) the d-band center decreases monotonically and significantly from −1.49 eV for Pt_1 via −1.65 eV and −1.72 eV for Pt_2 and Pt_3, respectively, towards that of the pure Pt(111) surface (−2.07 eV), these shifts are much smaller and less continuous for Pd_xAg_{1-x}/Pd(111). In the latter surface alloy, the center of the d-band is at around −1.34 eV for Pd_1 and Pd_2, and at −1.30 eV for the Pd_3 trimer, while it is at −1.53 eV for Pd(111) [22]. Hence, there is little difference in the d-band center in Pd_xAg_{1-x}/Pd(111) for the different small ensembles, and also the up-shift towards the Fermi level compared with Pd(111) is much smaller, only around 0.24 eV, than observed for Pt_xAg_{1-x}/Pt(111), where this shift amounts to ~0.6 eV. Thus, in agreement with the experimental findings, the calculations predict that the strengthening of the CO adsorption bond is much larger for Pt_xAg_{1-x}/Pt(111) than for Pd_xAg_{1-x}/Pd(111) surface alloys. This also explains the formation of the high temperature CO desorption peak for Pt_xAg_{1-x}/Pt(111), which is unique among these different surface alloys. While the exact reason for this unique behavior of the Pt_xAg_{1-x}/Pt(111) system could not be rationalized from the DFT calculations, the shifts of the center of the d-band upon Ag addition as well as the calculated CO adsorption energies of the PtAg mixed layers clearly reproduce the trend observed experimentally. The physical origin of these distinct differences can only be speculated upon at present, as Pt and Pd have a very similar band structure as bulk materials.

The results of this systematic study on the interaction of CO with Pt_xAg_{1-x}/Pt(111) surface alloys and, in a more general sense, with a group of closely related Pt(111)- and Pd(111)-based surface alloys with Ag and Au, respectively, perfectly demonstrate the detail of atomic scale understanding of adsorption phenomena on bimetallic surfaces that can be gained from such studies. It furthermore illustrates not only the potential but also the limits of simple approximations such as the concept of constant bond order for estimating the direction of electronic ligand effects. Its limits become evident in the assessment of the

Please cite this article as: K.M. Schüttler, et al., Interaction of CO with PtxAg1−x/Pt(111) surface alloys: More than dilution by Ag atoms, Surf. Sci. (2015), http://dx.doi.org/10.1016/j.susc.2015.12.022

vertical ligand effects, which were expected to be stabilizing, but are actually found to be destabilizing in calculations, both for Pt_xAg_{1-x}/Pt(111) and Pd_xAg_{1-x}/Pd(111) surface alloys. While an assessment of the combined action of strain and ligand effect is possible already on the basis of such qualitative concepts for the case that they are working in the same direction, this is hardly possible without calculations for the opposite case of counteracting effects. In this case it is almost impossible to make an a priori statement which effect will prevail, i.e., whether destabilizing strain effects or stabilizing ligand effects will dominate or whether both will essentially cancel out. Here improved but nevertheless simple concepts would be highly desirable. This is important not only to better understand adsorption on bimetallic surfaces, but also to gain simple access to catalytic activities, by combining these trends in adsorption energies with modern concepts to describe catalytic activities involving the use of scaling laws and of the Sabatier principle.

5. Conclusion

In an effort to better understand trends in the interaction of adsorbates with bimetallic surfaces, and in the long run also trends in catalytic activities, we have systematically studied the interaction of CO with structurally well-defined Pt_xAg_{1-x}/Pt(111) surface alloys, combining experimental (TPD and IR measurements) and theoretical (DFT calculations) methods, and compared the resulting trends with those determined in previous studies on closely related Pt(111)- and Pd(111)-based surface alloys with the coinage metals Ag and Au. Based on this we arrived at the following conclusions:

(1) Neighboring Ag surface atoms (Ag ligands) strongly stabilize the CO adsorption on Pt surface atoms. Stabilizing ligand effects in the bimetallic layer overcompensate destabilizing strain effects caused by the compressively strained pseudomorphic PtAg surface alloy layer. This is shown both experimentally by TPD and IR results, as well as by DFT calculations.
(2) While this stabilization is weak for lower Ag contents and only reflected by an up-shift of the trailing edge to higher temperatures, it results in a distinct new desorption peak at higher temperature (~550 K) for surface alloys with more than 50% Ag content. Desorption in this peak is attributed to non-interacting CO_{ad} species adsorbed on Pt surface atoms with at least 4 Ag neighbors. This assignment is based on the absence of repulsive interactions in this feature with increasing total CO_{ad} coverage (as judged from TPD results), the sharpness of the corresponding IR band, the abundance of the respective Pt structures, and DFT calculations.
(3) Based on calculations, Ag in the sub-surface region will destabilize CO adsorption on Pt surface sites, in contrast to expectations based on the simple constant bond order concepts. A similar trend was reported previously for CO adsorption on Pd_xAg_{1-x}/Pd(111).
(4) The stabilization of CO adsorbed on a Pt surface atom surrounded by (mostly) Ag surface atoms is unique for Pt_xAg_{1-x}/Pt(111) surface alloys and has not been observed for other Pt(111)- or Pd(111)-based surface alloys with Ag/Au as second component. This agrees with predictions from the d-band model considering the up-shift of the d-band center.
(5) CO adsorption on Ag (step) defect sites, which is possible at temperatures 130–140 K, is stabilized by interaction of the Ag surface atoms with the Pt(111) substrate as compared with adsorption on similar defect sites on Ag(111). For a full Ag surface layer on Pt(111), a similar stabilization of CO adsorption has not been observed in the calculations.
(6) For CO adsorption on Pt(111)-based surface alloys ensemble effects are negligible. Similar to adsorption on Pt(111), CO adsorption is most stable in on-top sites. In contrast, for Pd(111)-based surface alloys the CO adsorption energy is determined by ensemble effects, with adsorption in threefold sites as provided by compact Pd_3 trimers being most stable, while on-top adsorption, which is possible already on Pd_1 monomers, is least stable.
(7) The above ensemble effects in combination with the almost statistical distribution of surface atoms result in a considerable upshift of the average adsorption energy/desorption temperature with decreasing coinage metal content for Pd(111)-based surface alloys. For CO/Pt_xAg_{1-x}/Pt(111), the upshift with increasing Pt content is less pronounced, except for the formation of the high temperature desorption peak. It originates from the pronounced stabilization arising from the combination of ligand and strain effects rather than from ensemble effects. For CO/Pt_xAu_{1-x}/Pt(111), where ensemble effects are equally absent, ligand and strain effect essentially cancel out, and the CO adsorption energy is almost independent of the Au surface content.
(8) CO molecules impinging on Ag sites, where stable adsorption is not possible at 100 K, can diffuse to neighboring free Pt sites up to Ag contents of 50%, as evidenced by the almost invariant initial sticking coefficient. Similar effects are indicated also for the other Pt(111)- and Pd(111)-based surface alloys.

In total, this series of studies has provided detailed insight and understanding, on a molecular scale level, into adsorption on bimetallic surfaces and the different effects contributing.

Acknowledgments

This work was supported by the Deutsche Forschungsgemeinschaft via the Research Unit 1376 (projects BE 1201/18-2 and GR 1503/22-2) and by the State Foundation of Baden-Württemberg via the Competence Network Functional Nanostructures (project B1). Q10

Appendix A. Supplementary data

Supplementary data to this article can be found online at http://dx.doi.org/10.1016/j.susc.2015.12.022.

References

[1] J.H. Sinfelt, Acc. Chem. Res. 10 (1977) 15.
[2] J.H. Sinfelt, Bimetallic Catalysts: Discoveries, Concepts and Applications, Wiley, New York, 1983.
[3] C.T. Campbell, Annu. Rev. Phys. Chem. 41 (1990) 775.
[4] V. Ponec, Appl. Catal. A 222 (2001) 31.
[5] Y. Soma-Noto, W.M.H. Sachtler, J. Catal. 34 (1974) 162.
[6] J.W.A. Sachtler, G.A. Somorjai, J. Catal. 81 (1983) 77.
[7] R.T. Vang, K. Honkala, S. Dahl, E. Kruse Vestergaard, J. Schnadt, E. Laegsgaard, B.S. Clausen, J.K. Nørskov, F. Besenbacher, Nat. Mater. 4 (2005) 160.
[8] V. Ponec, W.M.H. Sachtler, J. Catal. 24 (1972) 250.
[9] W.M.H. Sachtler, Le Vide 164 (1973) 67.
[10] W.M.H. Sachtler, in: G. Ertl, H. Knözinger, J. Weitkamp (Eds.), Handbook of Heterogeneous Catalysis, vol. 3, VCH-Wiley, Weinheim, 1997.
[11] M. Mavrikakis, B. Hammer, J.K. Nørskov, Phys. Rev. Lett. 81 (1998) 2819.
[12] B. Hammer, J.K. Nørskov, Adv. Catal. 45 (2000) 71.
[13] M. Chen, D. Kumar, C.-W. Yi, D.W. Goodman, Science 310 (2005) 291.
[14] A. Logadottir, T.H. Rod, J.K. Nørskov, B. Hammer, S. Dahl, C.J.H. Jacobsen, J. Catal. 197 (2001) 229.
[15] F. Abild-Pedersen, J. Greeley, J. Rossmeisl, F. Studt, T.R. Munter, P.G. Moses, E. Skúlason, T. Bligaard, J.K. Nørskov, Phys. Rev. Lett. 99 (2007) 016105.
[16] G. Jones, T. Bligaard, F. Abild-Pedersen, J.K. Nørskov, J. Phys. Condens. Matter 20 (2008) 064239.
[17] S. Brimaud, A.K. Engstfeld, O.B. Alves, H.E. Hoster, R.J. Behm, Top. Catal. 57 (2014) 222.
[18] S. Brimaud, A.K. Engstfeld, O.B. Alves, R.J. Behm, J. Electroanal. Chem. 716 (2014) 71.
[19] M. Ruff, N. Takehiro, P. Liu, J.K. Nørskov, R.J. Behm, ChemPhysChem 8 (2007) 2068.
[20] Y. Ma, J. Bansmann, T. Diemant, R.J. Behm, Surf. Sci. 603 (2009) 1046.
[21] Y. Ma, T. Diemant, J. Bansmann, R.J. Behm, Phys. Chem. Chem. Phys. 13 (2011) 10741.
[22] L.A. Mancera, R.J. Behm, A. Groß, Phys. Chem. Chem. Phys. 15 (2013) 1497.
[23] M. Eyrich, T. Diemant, H. Hartmann, J. Bansmann, R.J. Behm, J. Phys. Chem. C 116 (2012) 11154.
[24] N. Takehiro, P. Liu, A. Bergbreiter, J.K. Nørskov, R.J. Behm, Phys. Chem. Chem. Phys. 16 (2014) 23930.
[25] A.K. Engstfeld, H.E. Hoster, R.J. Behm, Phys. Chem. Chem. Phys. 14 (2012) 10754.
[26] A. Bergbreiter, O.B. Alves, H.E. Hoster, ChemPhysChem 11 (2010) 1505.

Please cite this article as: K.M. Schüttler, et al., Interaction of CO with PtxAg1−x/Pt(111) surface alloys: More than dilution by Ag atoms, Surf. Sci. (2015), http://dx.doi.org/10.1016/j.susc.2015.12.022

[27] R. Rötter, Diploma Thesis, Ulm University, 2009.
[28] T. Diemant, K.M. Schüttler, R.J. Behm, ChemPhysChem 16 (2015) 2943.
Q12 [29] R. Rötter, L.A. Mancera, A. Groß, R.J. Behm, 2015 to be published.
[30] H. Röder, R. Schuster, H. Brune, K. Kern, Phys. Rev. Lett. 71 (1993) 2086.
[31] U. Strüber, J. Küppers, Surf. Sci. 294 (1993) L924.
[32] H. Hopster, H. Ibach, Surf. Sci. 77 (1978) 109.
[33] H. Steininger, S. Lehwald, H. Ibach, Surf. Sci. 123 (1982) 264.
[34] P. Feulner, D. Menzel, J. Vac. Sci. Technol. 17 (1980) 662.
[35] V.S. Smentkowski, J.T. Yates Jr., J. Vac. Sci. Technol. A 7 (1989) 3325.
[36] G. Kresse, J. Furthmüller, Phys. Rev. B 54 (1996) 11169.
[37] J.P. Perdew, K. Burke, M. Ernzerhof, Phys. Rev. Lett. 77 (1996) 3865.
[38] B. Hammer, L.B. Hansen, J.K. Nørskov, Phys. Rev. B 59 (1999) 7413.
[39] P.E. Blöchl, Phys. Rev. B 50 (1994) 17953.
[40] G. Kresse, D. Joubert, Phys. Rev. B 59 (1999) 1758.
[41] G. Kresse, J. Furthmüller, Comput. Mater. Sci. 6 (1996) 15.
[42] R.W.G. Wyckoff, Crystal Structures, vol. 1, Interscience Publ., New York, 1963.
[43] L.Z. Mezey, J. Giber, Jpn. J. Appl. Phys. 21 (1982) 1569.
[44] E. Habenschaden, J. Küppers, Surf. Sci. 138 (1984) L147.
[45] P.A. Redhead, Vacuum 12 (1962) 203.
[46] G. Ertl, M. Neumann, K.M. Streit, Surf. Sci. 64 (1977) 393.
[47] B.E. Hayden, A.M. Bradshaw, Surf. Sci. 125 (1983) 787.
[48] J.L. Gland, E.B. Kollin, J. Chem. Phys. 78 (1983) 963.
[49] M.T. Paffett, S.C. Gebhard, R.G. Windham, B.E. Koel, J. Phys. Chem. 94 (1990) 6831.
[50] J.-S. McEwen, S.H. Payne, H.J. Kreuzer, M. Kinne, R. Denecke, H.P. Steinrück, Surf. Sci. 545 (2003) 47.
[51] W. Hansen, M. Bertolo, K. Jacobi, Surf. Sci. 253 (1991) 1.
[52] J. Lee, J.-G. Lee, J.T. Yates Jr., Surf. Sci. 594 (2005) 20.
[53] C.T. Campbell, G. Ertl, H. Kuipers, J. Segner, Surf. Sci. 107 (1981) 207.
[54] P.J. Kisliuk, J. Phys. Chem. Solids 3 (1957) 95.
[55] H. Hartmann, T. Diemant, J. Bansmann, R.J. Behm, Surf. Sci. 603 (2009) 1456.
[56] H. Pfnür, D. Menzel, J. Chem. Phys. 79 (1983) 2400.
[57] C. Xu, B.E. Koel, Surf. Sci. 304 (1994) L505.
[58] P. Hollins, Surf. Sci. Rep. 16 (1992) 51.
[59] C.W. Olsen, R.I. Masel, Surf. Sci. 201 (1988) 444.
[60] E. Schweizer, B.N.J. Persson, M. Tüshaus, D. Hoge, A.M. Bradshaw, Surf. Sci. 213 (1989) 49.
[61] B.N.J. Persson, J. Chem. Phys. 92 (1990) 5034.
[62] M. Tüshaus, W. Berndt, H. Conrad, A.M. Bradshaw, B.N.J. Persson, Appl. Phys. A Mater. Sci. Process. 51 (1990) 91.
[63] N. Kizhakevariam, X. Jiang, M.J. Weaver, J. Chem. Phys. 100 (1994) 6750.
[64] M. Andersen, M. Johansson, I. Chorkendorff, J. Phys. Chem. B 109 (2005) 10285.
[65] G. Blyholder, J. Phys. Chem. 68 (1964) 2772.
[66] P.J. Feibelman, B. Hammer, J.K. Nørskov, F. Wagner, M. Scheffler, R. Stumpf, R. Watwe, J. Dumesic, J. Phys. Chem. B 105 (2001) 4018.
[67] I. Grinberg, Y. Yourdshahyan, A.M. Rappe, J. Chem. Phys. 117 (2002) 2264.
[68] R.A. Olsen, P.H.T. Philipsen, E.J. Baerends, J. Chem. Phys. 119 (2003) 4522.
[69] Y. Wang, S. de Gironcoli, N.S. Hush, J.R. Reimers, J. Am. Chem. Soc. 129 (2007) 10402.
[70] L. Schimka, J. Harl, A. Stroppa, A. Grüneis, M. Marsman, F. Mittendorfer, G. Kresse, Nat. Mater. 9 (2010) 741.
[71] Y. Gohda, A. Groß, Surf. Sci. 601 (2007) 3702.
[72] A. Roudgar, A. Groß, J. Electroanal. Chem. 548 (2003) 121.
[73] B. Hammer, Y. Morikawa, J.K. Nørskov, Phys. Rev. Lett. 76 (1996) 2141.
[74] J.A. Rodriguez, C.M. Truong, D.W. Goodman, Surf. Sci. 271 (1992) L331.
[75] A. Groß, J. Phys. Condens. Matter 21 (2009) 084205.
[76] F. Calle-Vallejo, J.I. Martínez, J.M. García-Lastra, J. Rossmeisl, M.T.M. Koper, Phys. Rev. Lett. 108 (2012) 116103.
[77] H. Xin, A. Vojvodic, J. Voss, J.K. Nørskov, F. Abild-Pedersen, Phys. Rev. B 89 (2014) 115114.
[78] P. Dumas, R.G. Tobin, P.L. Richards, Surf. Sci. 171 (1986) 555.
[79] P. Liu, J.K. Nørskov, Phys. Chem. Chem. Phys. 3 (2001) 3814.
[80] A.M. Bradshaw, F.M. Hoffmann, Surf. Sci. 72 (1978) 513.
[81] F.M. Hoffmann, Surf. Sci. Rep. 3 (1983) 107.
[82] Y. Gohda and A. Groß, unpublished.

Please cite this article as: K.M. Schüttler, et al., Interaction of CO with PtxAg1−x/Pt(111) surface alloys: More than dilution by Ag atoms, Surf. Sci. (2015), http://dx.doi.org/10.1016/j.susc.2015.12.022